Dynamics and critical behavior of the *q* model

Marta Lewandowska,[1] H. Mathur,[1] and Y.-K. Yu[2]

[1]*Department of Physics, Case Western Reserve University, Cleveland, Ohio 44106-7079*
[2]*Department of Physics, Florida Atlantic University, Boca Raton, Florida 33431*
(Received 6 July 2000; published 18 July 2001)

The *q* model, a random walk model rich in behavior and applications, is investigated. We introduce and motivate the *q* model via its application proposed by Coppersmith *et al.* to the flow of stress through granular matter at rest. For a special value of its parameters the *q* model has a critical point that we analyze. To characterize the critical point we imagine that a uniform load has been applied to the top of the granular medium and we study the evolution with depth of fluctuations in the distribution of load. Close to the critical point explicit calculation reveals that the evolution of load exhibits scaling behavior analogous to thermodynamic critical phenomena. The critical behavior is remarkably tractable: the harvest of analytic results includes scaling functions that describe the evolution of the variance of the load distribution close to the critical point and of the entire load distribution right at the critical point, values of the associated critical exponents, and determination of the upper critical dimension. These results are of intrinsic interest as a tractable example of a random critical point. Of the many applications of the *q* model, the critical behavior is particularly relevant to network models of river basins, as we briefly discuss. Finally we discuss circumstances under which quantum network models that describe the surface electronic states of a quantum Hall multilayer can be mapped onto the classical *q* model. For mesoscopic multilayers of finite circumference the mapping fails; instead a mapping to a ferromagnetic supersymmetric spin chain has proved fruitful. We discuss aspects of the superspin mapping and give an elementary derivation of it making use of operator rather than functional methods.

I. INTRODUCTION

It is fortunate that in physics the same equations sometimes arise in contexts that are apparently very different. Feynman illustrates this through elementary examples in his introductory lectures on physics to impart the lesson that the "same equations have the same solutions" [1]. Our purpose is to study a model, recently dubbed the *q* model, that provides another such instance. The *q* model has been used to describe the merging of tributaries to form rivers [2]; the aggregation of diffusing charges [3]; the flow of stress in a granular medium [4]; and can be mapped onto the abelian sandpile, a model studied in context of self-organized criticality [5]. It is also closely related to models that describe the surface of a quantum Hall multilayer [6,7] and passive scalar turbulence [8,9]. Here we focus on the application to granular matter, river networks, and the quantum Hall multilayer.

Granular matter exhibits fascinating behavior that is little understood [10]. Examples of granular matter include sand, powders, and agricultural grains stored in silos. An important problem is the propagation of stress through a granular medium at rest. This has been studied by ingenious experiments, in which a vertical load is applied to an amorphous pack of beads, and the loads on the beads in the top and bottom layers are recorded using carbon paper [11,12]. Such experiments yield the distribution of load on the beads and reveal that there are no horizontal correlations in load even amongst neighboring beads. The *q* model was introduced by Coppersmith *et al.* to account for the distribution of load [4]. As we shall see, it also correctly predicts the lack of horizontal correlation.

For simplicity we describe the *q* model in a plane. Since the vertical and horizontal directions are treated asymmetri-

cally we call this the $1+1$ dimensional *q* model. The extension to $2+1$ dimensions (relevant to experiments on bead packs) and higher, is straightforward and is discussed in Sec. V. In the *q* model it is assumed that the beads sit on a regular lattice shown in Fig. 1. The location of the beads is specified by the coordinates *t* (the depth of the layer) and *n* (the location of the bead within the layer). Note that *n* takes only even values for *t* even; only odd, for *t* odd. Each bead is assumed to be supported by its two nearest neighbors in the layer directly below. More precisely, it is assumed that a random fraction $f_n(t)$ of the load of bead (n,t) is supported by the neighbor to the left, bead $(n-1,t+1)$; the remainder, $1-f_n(t)$, by the neighbor to the right, bead $(n+1,t+1)$. Denoting the load on a bead *w* and its weight *I* we may write

$$w_n(t) = w_{n-1}(t-1)[1-f_{n-1}(t-1)]$$
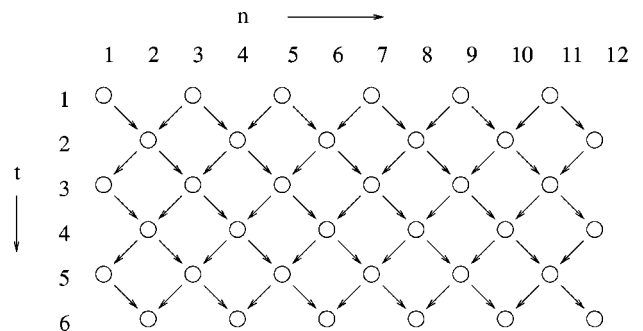$$+ w_{n+1}(t-1)f_{n+1}(t-1) + I_n(t). \quad (1)$$

FIG. 1. The *q* model of stress propagation through a bead pack in $1+1$ dimensions. The beads are assumed to sit on a regular lattice. Each bead is supported by its two nearest neighbors in the layer below.

The content of Eq. (1) is that the load on a bead is the sum of the loads transmitted to it by its neighbors in the layer above plus its own weight. The last term in Eq. (1) is called the injection term. Once the fractions are specified, a given load on the top layer can be propagated downward by use of Eq. (1).

In the q model it is assumed that the fractions are independent, identically distributed random variables. The distribution is assumed to be symmetric about $f = 1/2$ to avoid introducing a horizontal drift to the flow of stress; in other words it is assumed $P(f) = P(1 - f)$. There is no other restriction. Thus the q models really constitute an enormous family of models corresponding to different symmetric distributions $P(f)$. To fully specify a particular model it is necessary to choose the distribution $P(f)$. One obvious possibility is to take $P(f)$ to be uniformly distributed over the unit interval; another is to assume that the fractions must be 0 or 1 with equal probability. The latter is called the singular distribution.

Mathematically, the q model is a problem of random walkers that coalesce upon contact and fission spontaneously. The singular distribution corresponds to the case that the walkers coalesce but do not fission.

Coppersmith *et al.* argued that, neglecting injection, at sufficient depth the distribution of load would attain a steady state [4]. They studied $\Pi(w, t \to \infty)$, the probability distribution of load on beads in a sufficiently deep layer. For almost all distributions $P(f)$, except the singular distribution, it was concluded that $\Pi(w, t \to \infty)$ decays exponentially for large w [4,15]. This agrees with experiment and constitutes an important success of the q model. For the singular distribution, Coppersmith *et al.* argued that $\Pi(w, \infty)$ follows a power law. Hence they conjectured that the singular distribution constitutes a critical point in the family of q models. A major goal of this paper is to make this analogy to thermodynamic critical phenomena precise by detailed analysis of the critical point.

In spite of the success mentioned above the q model cannot be considered a complete theory of stress propagation in granular matter. This is clear both empirically and on grounds of internal consistency. Since the publication of the q model, interesting new ideas on the subject of stress flow have appeared [8,13–15], but in this paper we restrict attention to the q model. This seems justified because the q model does capture some elements of the physics correctly and because it exhibits nontrivial critical behavior that is interesting in its own right.

Further motivation to study the q model and particularly its critical point comes from hydrology. To make contact with that subject consider a singular q model with zero injection and imagine that only a few beads in the top layer are loaded. The load then zigzags downwards, perhaps along the lines shown in Fig. 2. If we interpret these lines as tributaries merging to form a river we arrive at Scheidegger's model [2] that appeared in the hydrology literature more than thirty
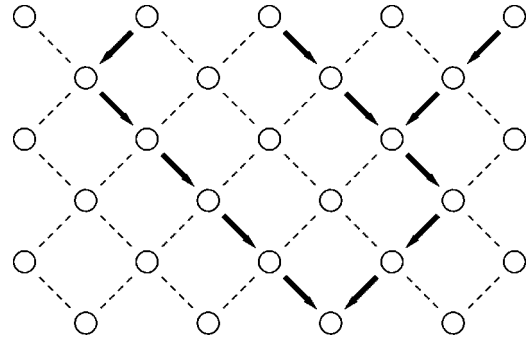

FIG. 2. *Scheidegger's model:* For the singular q model the load zigzags down lines that merge but do not split. In Scheidegger's model of river basins these lines are interpreted as tributaries merging to form a river.

years ago.[1] Networks of tributaries in river basins are known empirically to be scale invariant structures that obey a variety of power laws. Scheidegger networks too obey these laws and are in this statistical sense extremely realistic representations of river basins. An excellent discussion of river basin power laws is given in Refs. [18,19]. Reference [18] presents some discussion of data; Ref. [19] provides a detailed comparison between real and Scheidegger networks.

Here we wish to point out that nonsingular q models too can be interpreted as models of river networks. For example, consider a model in which the fractions can take only the values 0, 1/2, and 1 with probability $(1 - \delta)/2$, δ, and $(1 - \delta)/2$, respectively. This model reduces to Scheidegger's as $\delta \to 0$. It produces networks similar to Scheidegger's except that occasionally streams split to form distributaries. Thus this network is topologically distinct from Scheidegger networks. More significantly, as we show below, a network with nonzero δ is not scale invariant. This is reminiscent of a river network model studied by Narayan and Fisher [20]. In their "rocky-river" model too the network is not scale invariant except if a model parameter is tuned to a special (critical) value. Effectively this tuning parameter also controls river splitting. Taken together, these results suggest that river splitting is a relevant perturbation that spoils the scale invariant structure of networks. In this paper we concentrate on showing that q-model networks with river splitting are not scale invariant. We do not explore whether such nonscale invariant networks are realized in nature (for further discussion and speculation in this regard, however, see Sec. VII).

A quantum Hall multilayer consists of layers of two-dimensional electron gases stacked vertically. Multilayers

---

[1]Parenthetically we note that Scheidegger's model is purely descriptive in the sense that it is a recipe to draw statistically realistic networks. Somewhat different in spirit are models that seek to represent physical processes, sometimes very crudely, by which the network forms. Two examples of such models in the recent physics literature are Refs. [16,17]. The model of Leheny and Nagel for example describes an apocalyptic lattice world with discrete time. Each time step brings precipitation, and in its wake, erosion and avalanches. Realistic networks result.
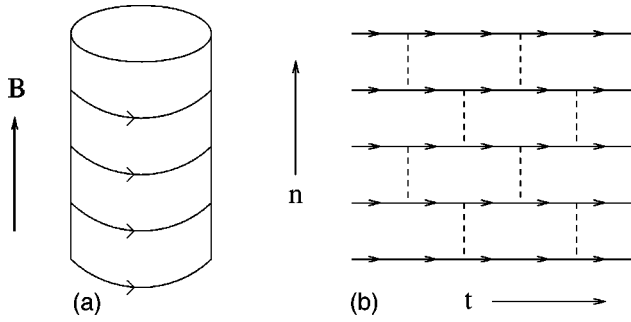
FIG. 3. *A quantum Hall multilayer:* Layers of two-dimensional electron gases are stacked vertically and a strong perpendicular magnetic field is applied. The important electronic states are at the edge of each layer. These chiral edge states propagate in the direction shown in (a). A quantum network model for the surface of the multilayer is shown in (b).

can be realized by fabricating an appropriate GaAs heterostructure [21]. They are also realized naturally in some organic salts. In a quantum Hall multilayer a sufficiently large magnetic field is applied perpendicular to the layers so that the lowest Landau level in each layer is fully occupied. Under this circumstance the only important electronic states in each layer are the chiral edge states that propagate in one direction only as shown in Fig. 3(a). These edge states are coupled by tunneling between layers. Thus the surface of a multilayer is covered by a chiral sheath of coupled edge states. These surface states control the electrical transport properties of the multilayer. A central question from a quantum transport point of view is whether these surface states are localized or extended in the direction of the field [7,22,23].

Figure 3(b) shows a network model of the multilayer surface introduced by Saul, Kardar, and Read [6] and studied by many authors subsequently. In this model it is assumed that tunneling between edges takes place only at discrete nodes [dashed vertical lines in Fig. 3(b)] that appear at regular intervals along an edge. The edges are separated by nodes into horizontal segments called links. The wave function has a definite value on each link. Each node is visited by two incoming links and by two outgoing links. Each node is characterized by a 2×2 S matrix that relates the wave function on the outgoing links to the incoming amplitudes. Once the S matrices are specified, given the wave function through a vertical slice, we can propagate it to the right. The S matrices are chosen at random from some ensemble to incorporate the effect of disorder. To fully specify the model it is necessary to choose a distribution for the S matrices. Periodic boundary conditions are imposed in the horizontal direction [7].

The directed network model above is quantum mechanical but in the limit of infinite circumference and for a special choice of disorder, Saul, Kardar, and Read have shown that it reduces to a *classical* model, the q model with uniform distribution of fractions and zero injection [6]. In Sec. VI we discuss some respects in which more generic models of the multilayer surface, that do not reduce to classical models, still do show behavior similar to the q model [24,25]. At the same time we show that in case of finite circumference quan-

tum interference effects become important and there is little to be learned from the study of the classical q model. Instead a mapping to a ferromagnetic supersymmetric spin chain has proved fruitful in this case [23,26]. In Sec. VI we discuss aspects of this mapping.

A detailed summary of our results is given in Sec. VII. The reader interested in first obtaining an overview of the paper or interested only in the results should proceed directly to Sec. VII.

II. CRITICAL BEHAVIOR IN 1+1 DIMENSIONS

Coppersmith *et al.* analyzed the distribution of load $\Pi(w,t\rightarrow\infty)$ at very large depth where presumably a steady state is achieved [4]. Here we study how the distribution evolves as a function of depth to this asymptotic steady state. We assume that a uniform load is applied to the top layer,

$$w_n(t)=1 \quad \text{for all } n. \tag{2}$$

In this section we neglect the weight of each bead (the injection term). In partial support of this neglect we note that in the experiment of Ref. [12] typically a total load of 7600 N was applied to the bead pack. In comparison we estimate that the weight of a single bead was less than a milliNewton; of the entire pack, less than 100 N. However, right at the critical point injection is a relevant perturbation, and at sufficiently large depth must be taken into account even if the weight of a single bead is small. We return to the effects of injection in Sec. IV.

To make the problem tractable we study not the entire distribution $\Pi(w,t)$ but only its lowest nontrivial moment. With the neglect of injection it follows that the total load on every layer is the same; the q-model dynamics [Eq. (1)] just shuffles this load. Hence the average load in layer t

$$\langle w(t)\rangle=\int_0^\infty dw\, w\Pi(w,t)$$

$$=1. \tag{3}$$

The lowest nontrivial moment is therefore the variance

$$\langle \delta w^2(t)\rangle=\int_0^\infty dw\, w^2\Pi(w,t)-1. \tag{4}$$

Since a uniform load is applied to the top layer the variance in that layer vanishes. As the load propagates downward, the fluctuations must grow and saturate. Our purpose is to analyze this evolution for different distributions $P(f)$, particularly those that are close to the singular distribution.

Right at the critical point the asymptotic distribution $\Pi(w,\infty)$ is believed to be a power law. If we assume that it does not have a well defined variance, then by analogy to critical phenomena we surmise that close to the critical point the variance must diverge as

$$\langle \delta w^2(t\rightarrow\infty)\rangle\sim\frac{1}{\delta^\theta}. \tag{5}$$

Here δ measures the distance of a distribution $P(f)$ from the singular distribution; δ will be defined precisely below. We also expect that the depth scale ξ_{corr} at which the steady state is attained will diverge as the critical point is approached. Thus

$$\xi_{\mathrm{corr}} \sim \frac{1}{\delta^{\varphi}}, \tag{6}$$

ξ_{corr} is a vertical correlation length that diverges as the critical point is approached. Combining Eqs. (5) and (6) we expect that close to the critical point the fluctuations must have a scaling form

$$\langle \delta w^2(t) \rangle = \frac{1}{\delta^{\theta}} \mathcal{F}(t \delta^{\varphi}). \tag{7}$$

To be consistent with Eq. (5) we expect that the scaling function $\mathcal{F}(u) \to \mathrm{const}$ as $u \to \infty$. For short times we expect that the system should behave as it would at the critical point. The δ dependence should cancel and so we expect $\mathcal{F}(u) \sim u^{\theta/\varphi}$ for $u \ll 1$ so that $\langle \delta w^2(t) \rangle \sim t^{\theta/\varphi}$ at the critical point.

In the remainder of this section we will confirm that Eq. (7) and these inferences are valid. We will determine the exponents θ and φ and the scaling function $\mathcal{F}(u)$.

As an aside to experts we note that it may have been more natural to name the exponents $\theta \to (3 - \tau)/\sigma$ and $\varphi \to \nu z$. These names follow from a more general scaling hypothesis for the entire distribution [Eq. (174)]. However in this section we have elected to make the more restricted hypothesis Eq. (7) and to give the exponents single letter names taking care to avoid common exponent names such as α, β, and ν.

Finally we should emphasize that although for definiteness we have assumed that a uniform load is applied to the top layer, it is easy to show that at sufficient depth, in the scaling limit, the dynamics of the load fluctuations are insensitive to the precise distribution of load applied to the top layer.

A. Disorder average

Consider the correlation function

$$c_m(t) = \frac{1}{N} \sum_n \langle w_n(t) w_{n+m}(t) \rangle. \tag{8}$$

We assume there are N beads in each layer and we impose periodic boundary conditions in the horizontal direction. Ultimately we are interested in taking $N \to \infty$. Note that m is even for both $t =$ even and $t =$ odd. In terms of the correlation function the variance is given by

$$\langle \delta w^2(t) \rangle = c_0(t) - 1. \tag{9}$$

The correlation function obeys a remarkably simple evolution equation [Eq. (15) below]. This equation can be solved by straightforward classical analysis; the exact formal solution is given by Eq. (38). Thus it is not difficult to obtain the

entire correlation function by this method and thereby obtain information on the horizontal correlation length; but here we present only a detailed analysis of the variance, related to the on-site correlation function via Eq. (9).

To analyze the evolution of the correlation function we write

$$c_m(t+1) = \frac{1}{N} \sum_n \langle w_n(t+1) w_{n+m}(t+1) \rangle$$

$$= \frac{1}{N} \sum_n \langle w_{n+1}(t) w_{n+m+1}(t) f_{n+1}(t) f_{n+m+1}(t) \rangle$$

$$+ \text{others}$$

$$= \frac{1}{N} \sum_n \langle w_{n+1}(t) w_{n+m+1}(t) \rangle \langle f_{n+1}(t) f_{n+m+1}(t) \rangle$$

$$+ \text{others}. \tag{10}$$

To obtain the second line of Eq. (10) we have used Eq. (1). Four terms result; we have written only one for illustration. To obtain the third line it is crucial to observe that $w_n(t)$ depends only on fractions in the layers above. It is not correlated with the fractions in layer t, allowing us to factorize the average as shown.

To perform the average we need information about the distribution $P(f)$. By symmetry for any choice of distribution

$$\langle f \rangle = \int_0^1 df \, f P(f) = \frac{1}{2}. \tag{11}$$

For the variance we write

$$\left\langle \left(f - \frac{1}{2} \right)^2 \right\rangle = \frac{\epsilon}{4}, \tag{12}$$

where ϵ is a parameter that characterizes the distribution $P(f)$. For example, $\epsilon = 1/3$ for the uniform distribution. For the singular distribution the parameter takes its maximum possible value $\epsilon = 1$. Since the fractions for different beads are assumed to be independently distributed we conclude

$$\langle f_n(t_1) f_m(t_2) \rangle = \frac{1}{4} + \frac{\epsilon}{4} \delta_{n,m} \delta_{t_1,t_2}. \tag{13}$$

Substituting Eq. (13) in Eq. (10) we obtain

$$c_m(t+1) = \left(\frac{1}{4} + \frac{\epsilon}{4} \delta_{m,0} \right) c_m(t) + \text{others}$$

$$= \left(\frac{1}{2} + \frac{\epsilon}{2} \delta_{m,0} \right) c_m(t) + \left(\frac{1}{4} - \frac{\epsilon}{4} \delta_{m,2} \right) c_{m-2}(t)$$

$$+ \left(\frac{1}{4} - \frac{\epsilon}{4} \delta_{m,-2} \right) c_{m+2}(t). \tag{14}$$

In the second line of Eq. (14) the other terms have been unveiled. Recall that m takes even integer values. It is convenient to replace $m \rightarrow m/2$ to obtain

$$c_m(t+1) = \left(\frac{1}{2} + \frac{\epsilon}{2} \delta_{m,0} \right) c_m(t) + \left(\frac{1}{4} - \frac{\epsilon}{4} \delta_{m,1} \right) c_{m-1}(t)$$

$$+ \left(\frac{1}{4} - \frac{\epsilon}{4} \delta_{m,-1} \right) c_{m+1}(t). \tag{15}$$

Equation (15) is the main result of this section. It governs the evolution of the correlation function. We wish to solve it subject to the initial condition

$$c_m(t \rightarrow 0) = 1 \quad \text{for all } m. \tag{16}$$

The initial condition follows from the definition of c_m [Eq. (8)] and the assumed uniform load on the top layer. Note that the distribution $P(f)$ enters the evolution equation only through the parameter ϵ. Since the parameter takes its maximum value $\epsilon = 1$ for the singular distribution we may define

$$\delta = 1 - \epsilon \tag{17}$$

as the distance of a distribution $P(f)$ from the critical point.

B. Scattering solution

It is easy to verify that a steady state solution to Eq. (15) is

$$c_0 = \frac{1}{1 - \epsilon},$$

$$c_n = 1 \quad \text{for } n \neq 0. \tag{18}$$

Assuming this is the unique steady state towards which our initial condition evolves, Eq. (18) reveals that the variance does diverge as the singular distribution is approached. Using Eq. (9)

$$\langle \delta^2 w(t \rightarrow \infty) \rangle = \frac{\epsilon}{1 - \epsilon}$$

$$\approx \frac{1}{\delta} \quad \text{as } \epsilon \rightarrow 1. \tag{19}$$

Comparing Eq. (5) we see that the exponent $\theta = 1$. Equation (18) also reveals that in steady state the fluctuations in load are uncorrelated for all pairs of beads including neighbors. This is in agreement with experiment [12].

A full solution of evolution dynamics needs more work. Schematically Eq. (15) states

$$c(t+1) = Hc(t). \tag{20}$$

The strategy we adopt here is to seek the eigenvectors of H,

$$H \phi^\lambda = \lambda \phi^\lambda, \tag{21}$$

and to expand the initial correlation vector $c(0)$ in terms of the eigenvectors,

$$c(0) = \sum_\lambda a_\lambda \phi^\lambda. \tag{22}$$

The correlation vector at depth t is then

$$c(t) = \sum_\lambda \lambda^t a_\lambda \phi^\lambda. \tag{23}$$

A complication we must negotiate is that H is non-Hermitian. According to the standard theory of biorthogonal expansion (briefly recounted in Appendix A) to execute the plan above we must *prove* that the eigenvectors of H span the vector space. Then we must find the eigenvectors of $H^\dagger$, called the left eigenvectors of H in this context. The eigenvalues of $H^\dagger$ are the complex conjugate of the eigenvalues of H. Thus

$$H^\dagger \psi^\lambda = \lambda^* \psi^\lambda, \tag{24}$$

where ψ^λ denotes the left eigenvector with eigenvalue λ^*. Having completed these tasks we may write the completeness relation

$$\sum_\lambda (\psi_m^\lambda)^* \phi_n^\lambda = \delta_{mn}. \tag{25}$$

Using Eq. (25) we conclude that the expansion coefficients in Eq. (22) are determined by the left eigenvectors,

$$a_\lambda = \sum_m (\psi_m^\lambda)^* c_m(0). \tag{26}$$

Implementing the plan we first write the eigenvalue equation for H

$$\frac{1}{2} \phi_r^\lambda + \frac{1}{4} \phi_{r+1}^\lambda + \frac{1}{4} \phi_{r-1}^\lambda = \lambda \phi_r^\lambda \quad \text{for } |r| \geq 2,$$

$$\frac{1}{2} \phi_{-1}^\lambda + \frac{1}{4} \phi_{-2}^\lambda + \frac{1-\epsilon}{4} \phi_0^\lambda = \lambda \phi_{-1}^\lambda,$$

$$\frac{1+\epsilon}{2} \phi_0^\lambda + \frac{1}{4} \phi_{-1}^\lambda + \frac{1}{4} \phi_1^\lambda = \lambda \phi_0^\lambda, \tag{27}$$

$$\frac{1}{2} \phi_1^\lambda + \frac{1-\epsilon}{4} \phi_0^\lambda + \frac{1}{4} \phi_2^\lambda = \lambda \phi_1^\lambda.$$

Note that for $\epsilon = 0$ Eq. (27) may be interpreted as the Schrödinger equation for a free particle on a tightbinding lattice, familiar from elementary solid state physics. For nonzero ϵ the particle may be viewed as scattering off a (non-Hermitian) barrier at the origin. Thus we seek a solution of the scattering form

$$\phi_n^{(+)k} = T(k) e^{ikn} \quad \text{for } n \geq 1,$$

$$= A(k) \quad \text{for } n = 0,$$

$$= e^{ikn} + R(k) e^{-ikn} \quad \text{for } n \leq -1. \tag{28}$$

Here $0 < k < \pi$. The first line of Eq. (27) then yields the eigenvalue

$$\lambda(k) = \frac{1}{2} + \frac{1}{2}\cos k. \qquad (29)$$

The next three lines yield the scattering coefficients

$$A(k) = \frac{i \sin k}{(1-\epsilon)e^{ik} + \epsilon - \cos k},$$

$$T(k) = (1-\epsilon)A(k), \qquad (30)$$

$$R(k) = (1-\epsilon)A(k) - 1.$$

There are also scattering solutions to Eq. (27) corresponding to the fictitious particle coming in from the right

$$\phi_n^{(-)k} = e^{-ikn} + R(k)e^{ikn} \quad \text{for } n \geq 1,$$

$$= A(k) \quad \text{for } n = 0,$$

$$= T(k)e^{-ikn} \quad \text{for } n \leq -1. \qquad (31)$$

By symmetry the scattering coefficients for this state are also given by Eq. (30).

There are no bound state solutions to Eq. (27). The scattering solutions we have found all have real eigenvalues. In principle, since H is non-Hermitian, complex eigenvalues are also possible. However, it turns out there are no solutions with complex eigenvalue that are biorthonormalizable. It will be seen that the scattering solutions we have found constitute a complete set.

The next step is to find the left eigenvectors that obey

$$\frac{1}{2}\psi_r^\lambda + \frac{1}{4}\psi_{r+1}^\lambda + \frac{1}{4}\psi_{r-1}^\lambda = \lambda\psi_r^\lambda \quad \text{for } |r| \geq 2,$$

$$\frac{1}{2}\psi_{-1}^\lambda + \frac{1}{4}\psi_{-2}^\lambda + \frac{1}{4}\psi_0^\lambda = \lambda\psi_{-1}^\lambda,$$

$$\qquad (32)$$

$$\frac{1+\epsilon}{2}\psi_0^\lambda + \frac{1-\epsilon}{4}\psi_{-1}^\lambda + \frac{1-\epsilon}{4}\psi_1^\lambda = \lambda\psi_0^\lambda,$$

$$\frac{1}{2}\psi_1^\lambda + \frac{1}{4}\psi_0^\lambda + \frac{1}{4}\psi_2^\lambda = \lambda\psi_1^\lambda.$$

Equation (32) is the transpose of Eq. (27). The left eigenvectors are

$$\psi_n^{(+)k} = T(k)e^{ikn} \quad \text{for } n \geq 1,$$

$$= A(k) \quad \text{for } n = 0,$$

$$= e^{ikn} + R(k)e^{-ikn} \quad \text{for } n \leq -1 \qquad (33)$$

and

$$\psi_n^{(-)k} = e^{-ikn} + \mathcal{R}(k)e^{ikn} \quad \text{for } n \geq 1,$$

$$= \mathcal{A}(k) \quad \text{for } n = 0,$$

$$= \mathcal{T}(k)e^{-ikn} \quad n \leq -1. \qquad (34)$$

The scattering coefficients are given by

$$\mathcal{A}(k) = \frac{i(1-\epsilon)\sin k}{(\epsilon - \cos k) + (1-\epsilon)e^{ik}},$$

$$\mathcal{T}(k) = \mathcal{A}(k), \qquad (35)$$

$$\mathcal{R}(k) = \mathcal{A}(k) - 1.$$

Having found the left and right eigenvectors, by analogy with Eq. (25), we now posit the completeness relation

$$\int_0^\pi \frac{dk}{2\pi}(\psi_m^{(+)k*}\phi_n^{(+)k} + \psi_m^{(-)k*}\phi_n^{(-)k}) = \delta_{mn}. \qquad (36)$$

The proof of this completeness relation, an important element of the analysis, is carried out in Appendix A.

The expansion of the initial correlation vector indicated schematically in Eq. (22) may now be written

$$c_m(0) = \int_0^\pi \frac{dk}{2\pi}[a^{(+)}(k)\phi_m^{(+)k} + a^{(-)}(k)\phi_m^{(-)k}]. \qquad (37)$$

The correlation vector at depth t is now

$$c_m(t) = \int_0^\pi \frac{dk}{2\pi}\lambda(k)^t[a^{(+)}(k)\phi_m^{(+)k} + a^{(-)}(k)\phi_m^{(-)k}] \qquad (38)$$

as previously shown schematically in Eq. (23).

The expansion coefficients $a(k)$, obtained using the completeness relation [Eq. (36)], are

$$a^{(+)}(k) = \sum_{n=-\infty}^{+\infty} c_n(0)\psi_n^{(+)k*},$$

$$a^{(-)}(k) = \sum_{n=-\infty}^{+\infty} c_n(0)\psi_n^{(-)k*}, \qquad (39)$$

as previously indicated schematically in Eq. (26). To ensure convergence of the sums in Eq. (39) we set $c_m(0) \to e^{-\eta|m|}$ and take $\eta \to 0$ at the end. Using Eqs. (33), (34), and (35) we perform the sums exactly to obtain

$$a^{(+)}(k) = a^{(-)}(k)$$

$$= \mathcal{A}(k)^* + 2\mathcal{A}(k)^* \frac{e^{-ik-\eta}}{1-e^{-ik-\eta}} + \left(\frac{e^{ik-\eta}}{1-e^{ik-\eta}} - \text{cc}\right)$$

$$= 2\pi\mathcal{A}(k)^*\delta(k) + [1-\mathcal{A}(k)^*]i\cot\frac{k}{2}. \qquad (40)$$

The last line of Eq. (40) is obtained by taking the limit $\eta \to 0$.

Substituting Eq. (40) in Eq. (38) and making use of Eqs. (28), (29), (30), (31), and (35) we finally obtain

$$c_0(t) = \frac{1}{1-\epsilon} - \frac{\epsilon}{\pi} \int_0^\pi dk \frac{\cos^{2(t+1)}(k/2)}{\epsilon^2 - (2\epsilon-1)\cos^2 k}. \quad (41)$$

Equation (41) is the exact expression for the evolution of $c_0(t)$ that we sought.

Finally we would like to reexpress Eq. (41) in terms of standard special functions. Some of the manipulations will prove useful later in the analysis of injection. Introduce the z transform

$$c_0(z) = \sum_{t=0}^{\infty} z^t c_0(t) = \frac{1}{1-\epsilon} \frac{1}{1-z}$$

$$- \frac{\epsilon}{\pi} \int_0^\pi dk \frac{\cos^2(k/2)}{\epsilon^2 - (2\epsilon-1)\cos^2(k/2)} \frac{1}{1-z\cos^2(k/2)}. \quad (42)$$

The k integral may now be performed[2] to yield

$$c_0(z) = \frac{1}{(1-\epsilon)(1-z)} - \frac{\epsilon^2}{(1-\epsilon)(2\epsilon-1)(1-\alpha(\epsilon)z)}$$

$$- \frac{\epsilon}{(1-2\epsilon)\sqrt{1-z}(1-\alpha(\epsilon)z)}. \quad (43)$$

For brevity $\alpha(\epsilon) = \epsilon^2/(2\epsilon-1)$. Upon inversion of the z transform (details relegated to Appendix B) we obtain

$$c_0(t) = \frac{1}{1-\epsilon} - \frac{1}{\pi\epsilon} \int_1^\infty dx (x-1)^{-1/2} \frac{1}{x^{t+1}} \left(x - \frac{2\epsilon-1}{\epsilon^2} \right)^{-1}. \quad (44)$$

Comparing an integral representation for the hypergeometric function [27]

$$F(a,b,c;s) = \frac{\Gamma(c)}{\Gamma(c-b)\Gamma(b)} \int_1^\infty dx (x-1)^{c-b-1}$$

$$\times x^{a-c}(x-s)^{-a}, \quad (45)$$

valid for $\mathrm{Re}\, c > \mathrm{Re}\, b > 0$ and $|s| < 1$, we conclude

$$\langle \delta w^2(t) \rangle = \frac{\epsilon}{1-\epsilon} - \frac{1}{\pi\epsilon} \frac{\Gamma(1/2)\Gamma(t+3/2)}{\Gamma(t+2)}$$

$$\times F\left(1, t+3/2, t+2; \frac{2\epsilon-1}{\epsilon^2} \right). \quad (46)$$

---

[2]Extend the range from 0 to 2π. Then use the standard trick for turning an angular integral into a contour integral around the unit circle in the ζ plane via the substitution $\zeta \to e^{ik}$. See, for example, [27], p. 409.
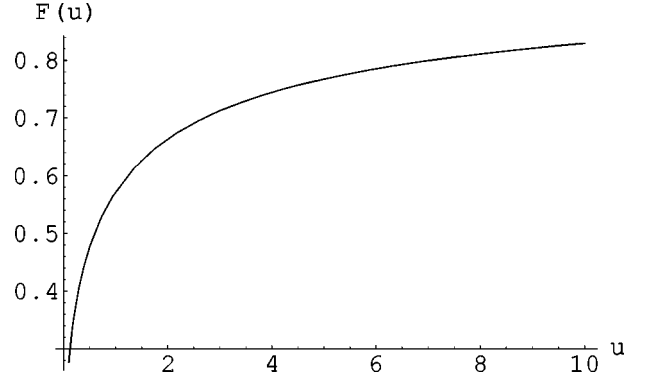

FIG. 4. The scaling function $\mathcal{F}(u)$ describes the growth of load fluctuations with depth for the $1+1$ dimensional q model close to the critical point [see Eqs. (7) and (50)]. Injection is neglected.

Equation (46) is the final result of this section. It is an exact formula for the evolution of fluctuations with depth, in terms of known special functions. As a practical matter Eqs. (41) and (44) are equivalent to Eq. (46) and will prove more useful.

C. Scaling limit

Equation (46) gives the exact evolution of load fluctuations for the q model without injection. It is valid for all t and all distributions, $P(f)$. From our point of view however it is more interesting to examine the scaling limit of large depth behavior near the critical point.

To derive the scaling limit we start with Eq. (44)—Eq. (41) would have served just as well—and consider the limit $t \gg 1$ and $\delta = 1 - \epsilon \to 0$. We do not make any assumption about the relationship between t and $1/\delta$. We obtain

$$\langle \delta^2 w(t) \rangle \approx \frac{1}{\delta} - \frac{1}{\pi} \int_0^\infty ds\, s^{-1/2} e^{-t\ln(1+s)} (s+\delta^2)^{-1}$$

$$\approx \frac{1}{\delta} - \frac{1}{\pi} \int_0^\infty ds\, s^{-1/2} e^{-ts} (s+\delta^2)^{-1}. \quad (47)$$

In the first line of Eq. (47) we have changed the integration variable from x to $s = x - 1$. Again changing the integration variable from s to $\bar{s} = s/\delta^2$ we obtain

$$\langle \delta^2 w(t) \rangle = \frac{1}{\delta} \left[1 - \frac{2}{\pi} \int_0^\infty d\bar{s} \frac{e^{-\bar{s}^2 t \delta^2}}{1+\bar{s}^2} \right]. \quad (48)$$

Comparing Eq. (7) we conclude that close to the critical point and in the large depth limit $\langle \delta^2 w(t) \rangle$ does indeed have a scaling form with exponents

$$\theta = 1, \quad \varphi = 2 \quad (49)$$

and scaling function

$$\mathcal{F}(u) = 1 - \frac{2}{\pi} \int_0^\infty ds \frac{e^{-us^2}}{1+s^2}. \quad (50)$$

Figure 4 shows a plot of $\mathcal{F}(u)$. As anticipated the asymptotic behavior of the scaling function is

$$\mathcal{F}(u) \approx 1 - \frac{1}{\sqrt{\pi u}} \quad \text{for} \quad u \to \infty$$

$$\approx \frac{2}{\sqrt{\pi}} \sqrt{u} \quad \text{for} \quad u \to 0. \tag{51}$$

We conclude that the saturation depth scale $\xi_{\text{corr}} \sim 1/\delta^2$. For very great depths $t \gg \xi_{\text{corr}}$, the fluctuations saturate to the value $1/\delta$ as found earlier by analysis of the steady state [Eq. (19)]. For small depths, $1 \ll t \ll \xi_{\text{corr}}$ they grow as

$$\langle \delta^2 w(t) \rangle = \frac{2}{\sqrt{\pi}} \sqrt{t}. \tag{52}$$

This behavior must persist at all depths right at the critical point as will be explicitly confirmed in Sec. III.

In summary, we have shown that the singular distribution is an isolated critical point in the space of q models. There is a (vertical) correlation length that diverges as the critical point is approached. We have determined the exponents θ and φ and the scaling function $\mathcal{F}(x)$ introduced in Eqs. (5), (6), and (7). In context of river networks we have found that any q model with stream splitting (hence nonzero δ) has a (possibly very long) correlation length in the direction of flow. Such a network is therefore not scale invariant on sufficiently long scales.[3]

III. CRITICAL POINT DISTRIBUTION

Right at the critical point in $1+1$ dimensions it is possible to analyze the dynamics of the entire distribution $\Pi(w,t)$. Since there is no vertical length scale at the critical point we expect that in the large depth, scaling limit

$$\Pi(w,t) = \frac{1}{t^\omega} \mathcal{H}(wt^\Upsilon). \tag{53}$$

Equation (53) implies that at the critical point the variance should grow as $t^{-3\Upsilon-\omega}$ in the scaling limit $t \gg 1$. From Eq. (7) we had surmised that the variance would grow as $t^{\theta/\varphi}$ for $\delta = 0$. Hence the exponents θ, φ of the preceding section and ω, Υ of this section are not independent; they satisfy the relation $3\Upsilon + \omega + \theta/\varphi = 0$. Below we calculate the exponents ω and Υ, explicitly verify the exponent relationship and obtain the scaling function $\mathcal{H}(s)$.

Again as an aside to experts we note that the exponents ω and Υ might more naturally have been written $\omega \to \tau/\nu z \sigma$, $\Upsilon \to -1/\nu z \sigma$. These expressions follow from the

---

[3]Strictly, to analyze a river network the appropriate initial condition is to load a fraction of randomly chosen sites in the $t=0$ layer, rather than the uniform load analyzed here. However we do not expect our conclusion regarding correlation lengths is sensitive to initial conditions.

$\delta \to 0$ limit of the more general scaling hypothesis for the entire distribution close to the critical point [Eq. (174)]. However for this section we have elected to make the more restricted hypothesis, Eq. (53), and to give the exponents single character names.

In this section too we neglect injection. At the critical point injection is a relevant perturbation. The form we derive is therefore a transient that will break down at sufficient depth. Provided the injection is weak however that depth could be very great.

Majumdar and Sire [28] have analyzed the scaling limit of $\Pi(w,t)$ when injection is present; however it does not appear straightforward to take the injection $\to 0$ limit in their expression. It would also be desirable for the case of nonzero injection to have a simple explicit formula for the crossover of $\Pi(w,t)$ from the transient we derive [Eq. (53)] to the injection dominated, large depth limit. Presumably this can be accomplished by extracting the suitable limit of the results of Ref. [28], or by direct calculation, but we do not attempt it here. The case of zero injection has also been previously analyzed by Majumdar and Huse in a continuum time model. Their results are in agreement with the scaling limit of our exact expression [29].

A. Disorder average

As in Sec. II we assume a uniform load is applied to the top layer [Eq. (2)]. To obtain the distribution $\Pi(w,t)$ following Ref. [3] we consider the quantities

$$Z_r(\rho,t) = \left\langle \exp i\rho \sum_{n=1}^{r} w_n(t) \right\rangle, \tag{54}$$

where $r = 1,2,3, \ldots$. By translational invariance

$$Z_1(\rho,t) = \langle \exp i\rho w_1(t) \rangle$$

$$= \sum_{w=0}^{\infty} e^{i\rho w} \Pi(w,t). \tag{55}$$

Note that for the critical q model without injection the load on a site is an integer. Thus $Z_1(\rho,t)$ is the discrete Fourier or z transform of the distribution $\Pi(w,t)$; ρ is the transform domain variable conjugate to w. $Z_2(\rho,t)$ similarly encodes the joint probability distribution of load on neighboring sites and so on.

For the business at hand the imaginary part of $Z_r(\rho,t)$,

$$\mathcal{Z}_r(\rho,t) = \text{Im} \, Z_r(\rho,t) \tag{56}$$

is especially valuable. It is evident from Eq. (55) that

$$\mathcal{Z}_1(\rho,t) = \sum_{w=0}^{\infty} \sin(\rho w) \Pi(w,t). \tag{57}$$

By using Fourier's identity

$$\frac{2}{\pi} \int_0^\pi dk \, \sin kn \, \sin km = \delta_{mn} \tag{58}$$

and Eq. (57) we can extract the distribution $\Pi(w,t)$ from $\mathcal{Z}_1(\rho,t)$ via

$$\Pi(w,t) = \frac{2}{\pi} \int_0^\pi d\rho \, \sin(\rho w) \mathcal{Z}_1(\rho,t) \qquad (59)$$

for $w = 1,2,3,\ldots$. We cannot obtain $\Pi(w=0,t)$ in this way from $\mathcal{Z}_1(\rho,t)$, but we can obtain it from the normalization of $\Pi(w,t)$;

$$\Pi(w\to 0,t) = 1 - \sum_{w=1}^\infty \Pi(w,t). \qquad (60)$$

The benefit of considering the quantities $Z_r(\rho,t)$ is that they obey a simple linear evolution equation. Following Ref. [3] write

$$Z_r(\rho,t+1) = \left\langle \exp i\rho \sum_{n=1}^r w_n(t+1) \right\rangle$$

$$= \left\langle \exp i\rho \left\{ w_1(t) f_1(t) + \sum_{n=2}^r w_n(t) \right. \right.$$

$$\left. \left. + w_{r+1}(t)[1 - f_{r+1}(t)] \right\} \right\rangle. \qquad (61)$$

To obtain the second line we have used the q-model evolution Eq. (1). Since the weights in layer t depend only on fractions in the preceding layers we can perform the average over $f_1(t)$ and $f_{r+1}(t)$ separately in Eq. (61):

$$\langle \exp i\rho w_1(t) f_1(t) \rangle_{f_1} = \frac{1}{2}[1 + \exp i\rho w_1(t)],$$

$$\langle \exp i\rho w_{r+1}(t)[1 - f_{r+1}] \rangle_{f_{r+1}} = \frac{1}{2}[1 + \exp i\rho w_{r+1}(t)]. \qquad (62)$$

Substituting Eq. (62) in Eq. (61) we obtain the evolution equation

$$Z_r(\rho,t+1) = \frac{1}{4} Z_{r-1}(\rho,t) + \frac{1}{2} Z_r(\rho,t) + \frac{1}{4} Z_{r+1}(\rho,t), \qquad (63)$$

where we have again made use of horizontal translational invariance.

Note that Eq. (63) is linear. Hence it is obeyed separately by the real and imaginary parts of Z. $\mathcal{Z}$ therefore evolves according to

$$\mathcal{Z}_r(\rho,t+1) = \frac{1}{4} \mathcal{Z}_{r-1}(\rho,t) + \frac{1}{2} \mathcal{Z}_r(\rho,t) + \frac{1}{4} \mathcal{Z}_{r+1}(\rho,t). \qquad (64)$$

Equation (64) is reminiscent of a tight-binding lattice Schrödinger equation for a free particle on a half line (since the site index $r \geq 1$).

The main results of this subsection are Eqs. (57) and (59) that define the relationship between $\Pi(w,t)$ and $\mathcal{Z}_1(\rho,t)$ and Eq. (64) that controls the evolution of $\mathcal{Z}_r(\rho,t)$ with depth.

B. Solution and scaling limit

We wish to solve Eq. (64) subject to the initial condition

$$\mathcal{Z}_r(\rho,t\to 0) = \sin \rho r. \qquad (65)$$

This follows from the assumed uniform load applied to the top layer and Eqs. (54) and (56). Schematically, Eq. (64) has the form

$$\mathcal{Z}_r(\rho,t+1) = \sum_s H_{rs} \mathcal{Z}_s(\rho,t). \qquad (66)$$

It is easy to verify that our initial condition is an eigenfunction of H;

$$\sum_s H_{rs} \sin \rho s = \left(\frac{1}{2} + \frac{1}{2} \cos \rho \right) \sin \rho r. \qquad (67)$$

Hence Eq. (64) has the remarkably simple solution

$$\mathcal{Z}_r(\rho,t) = \left(\frac{1}{2} + \frac{1}{2} \cos \rho \right)^t \sin \rho r. \qquad (68)$$

Substituting Eq. (68) in Eq. (59) we obtain the desired expression for

$$\Pi(w,t) = \frac{2}{\pi} \int_0^\pi d\rho \, \sin(\rho w) \left(\frac{1}{2} + \frac{1}{2} \cos \rho \right)^t \sin \rho \qquad (69)$$

for $w = 1,2,3,\ldots$.

The integral over ρ can be performed exactly by a standard contour integration trick (see footnote 2) to yield

$$\Pi(w,t) = \frac{1}{4^t} \frac{(2t)!}{(t+1-w)!(t-1+w)!}$$

$$- \frac{1}{4^t} \frac{(2t)!}{(t-1-w)!(t+1+w)!}$$

$$\text{for } w = 1,2,\ldots,t-1$$

$$= \frac{1}{4^t} \frac{(2t)!}{(t+1-w)!(t-1+w)!}$$

$$\text{for } w = t, t+1 = 0 \quad \text{for } w > t+1. \quad (70)$$

We now use Eqs. (60) and (70) to obtain $\Pi(w\to 0,t)$. The sum proves tractable and yields

$$\Pi(w\to 0,t) = 1 - \frac{1}{4^t} \frac{(2t+1)!}{(t+1)!t!}. \qquad (71)$$

Equations (70) and (71) are the exact expressions for $\Pi(w,t)$ for the critical q model without injection.

Much more interesting than the exact formula is the scaling limit of large depth. We now assume $t \gg 1$ but we will make no assumptions about the relative size of w and t. To derive this limit we return to Eq. (69) and write

$$\left(\frac{1}{2} + \frac{1}{2} \cos \rho \right)^t \approx e^{-t\rho^2/4} \tag{72}$$

justified (inside the integral) for large t. Hence we obtain a Gaussian integral

$$\Pi(w,t) = \frac{1}{\pi} \int_{-\pi}^{\pi} d\rho \, \sin(\rho w) \rho e^{-t\rho^2/4}$$

$$= \frac{4}{\sqrt{\pi}} \frac{w}{t^{3/2}} e^{-w^2/t}. \tag{73}$$

Comparing Eqs. (53) and (73) we see that at large depth Π has the anticipated scaling form with exponents

$$\omega = 1, \quad \Upsilon = -\frac{1}{2} \tag{74}$$

and scaling function

$$\mathcal{H}(s) = \frac{4}{\sqrt{\pi}} s e^{-s^2}. \tag{75}$$

Equation (73) holds for $w \gg 1$. In the same large depth limit

$$\Pi(w \to 0, t) \approx 1 - \frac{2}{\sqrt{\pi}} \frac{1}{\sqrt{t}}. \tag{76}$$

The distribution of load thus consists of a spike at zero load followed by smooth behavior for nonzero load given by Eq. (73). At great depths it is extremely probable that the load on a given bead is zero; most of the weight of the distribution is in the spike.

From the distribution of load, Eq. (73), it is easy to confirm that its variance [Eq. (4)] grows without bound as the square root of depth, as we had earlier inferred from the scaling function $\mathcal{F}$ [cf. Eq. (52)].

It is instructive that the exact formula, Eqs. (70) and (71), is so cumbersome; the scaling limit, Eqs. (53), (74), and (75), emerges only when we plumb the depths.

IV. EFFECT OF INJECTION

In this section we consider the q model in $1+1$ dimensions taking into account injection. We will assume that the weights of the beads are independent and identically distributed with mean $\langle I \rangle$ and variance $\langle \delta I^2 \rangle$. To probe the behavior of the model we will assume that a uniform load is applied to the top layer [Eq. (2)]. We will study how the mean square load $\langle w^2(t) \rangle$ evolves with depth since the mean load has the trivial variation

$$\langle w(t) \rangle = 1 + \langle I \rangle t. \tag{77}$$

Near the critical point we expect that the mean square load should have a scaling form

$$\langle w^2(t) \rangle = \frac{1}{\delta^\theta} \mathcal{C}(t \delta^\varphi, \langle \delta I^2 \rangle \delta^{-\mu}, \langle I \rangle \delta^{-\kappa}). \tag{78}$$

We can guess all the exponents and obtain some features of the scaling function from simple arguments. The load on a particular bead at depth t is a random linear combination of the weights of the beads in the layer above plus a term, due to the applied load, that does not depend on the weights, I_n. Hence the scaling function has to be of the form

$$\langle w^2(t) \rangle = \frac{1}{\delta^\theta} \mathcal{F}(t \delta^\varphi) + \frac{\langle \delta I^2 \rangle}{\delta^{\theta+\mu}} \mathcal{M}(t \delta^\varphi) + \frac{\langle I \rangle}{\delta^{\theta+\kappa}} \mathcal{K}(t \delta^\varphi)$$

$$+ \frac{\langle I \rangle^2}{\delta^{\theta+2\kappa}} \mathcal{L}(t \delta^\varphi). \tag{79}$$

In the limit of zero injection Eq. (79) should reduce to our result in Sec. II. Thus

$$\theta = 1, \quad \varphi = 2 \tag{80}$$

and $\mathcal{F}$ has the same form [Eq. (50)] as in Sec. II justifying the recycling of these particular symbols.

By rewriting the average weight at depth t [Eq. (77)] as $1 + t\delta^2 \langle I \rangle / \delta^2$ we conjecture

$$\kappa = 2. \tag{81}$$

To obtain μ we imagine that the system is very close to the critical point. Then for times that are not too long, effectively, it will behave as it would right at the critical point. At that point the weight of each bead zigzags down lines that merge but do not split. If we add the squares of the loads on all the beads on layer t we will obtain the sum, over all the beads above layer t, of their squared deviation from the average weight $\langle I \rangle$ plus other terms. Hence $\langle \Sigma_n w_n(t)^2 \rangle = \langle \delta I^2 \rangle N t +$ other pieces that do not depend on $\langle \delta I^2 \rangle$. Here N is the number of beads in a layer. By translational invariance we conclude

$$\langle w^2(t) \rangle \approx \langle \delta I^2 \rangle t + (\text{others}). \tag{82}$$

In Eq. (82) "others" represents contributions to $\langle w^2(t) \rangle$ that do not depend on $\langle \delta I^2 \rangle$. Comparing Eqs. (82) and (79) we see that for small values of its argument

$$\mathcal{M}(u) \approx u \tag{83}$$

and the exponent

$$\mu = 1, \tag{84}$$

needed to cancel the δ dependence at small depths.

With the exponents in hand we can analyze the behavior of $\langle w^2(t) \rangle$ at small depths (compared to $1/\delta^2$). This behavior would persist out to all depths right at the critical point. For the term independent of injection we have already obtained the exact result, Eq. (52). For the term that depends on $\langle \delta I^2 \rangle$

we have just worked out the behavior in this limit, including the precise coefficient [Eq. (82)]. For the term that is proportional to $\langle I \rangle$ we argue that for small u, $\mathcal{K}(u) \sim u^{3/2}$ to cancel the δ dependence, leading to

$$\langle w^2(t) \rangle \sim \langle I \rangle t^{3/2} + (\text{others}). \tag{85}$$

Similarly the contribution of the term that is proportional to $\langle I \rangle^2$ is

$$\langle w^2(t) \rangle \sim \langle I \rangle^2 t^{5/2} + (\text{others}). \tag{86}$$

The last result has a simple interpretation. We have seen in Sec. II that without injection at the critical point the mean weight at depth t is 1; the mean square weight $\sim \sqrt{t}$. With injection the average weight at sufficient depth is $\approx \langle I \rangle t$. If we assume that uniform injection does not change the distribution, only its scale, then since the mean is inflated by a factor $\langle I \rangle t$, the mean square should be inflated by a factor $\langle I \rangle^2 t^2$, leading to Eq. (86). The same interpretation can be used to derive the behavior of the last term in Eq. (79) in the limit $t \gg 1/\delta^2$, the opposite of the limit we have so far considered. In that limit, in the absence of injection, the fluctuations saturate at the value $1/\delta$. Hence we expect this term to behave as

$$\langle w^2(t) \rangle \sim \frac{1}{\delta} \langle I \rangle^2 t^2. \tag{87}$$

We can check some of these deductions by making contact with Majumdar and Sire, who have analyzed the entire distribution of load at the critical point [28]. Following these authors let us imagine that the injection term is very small, with the squared mean $\langle I \rangle^2$, significantly smaller than the variance $\langle \delta I^2 \rangle$. According to our analysis ultimately the fluctuations at the critical point should grow as $t^{5/2}$, but the depth at which the $t^{5/2}$ term [Eq. (86)] overtakes the term linear in t [Eq. (82)] could be very great; it diverges as $1/\langle I \rangle^{4/3}$. Majumdar and Sire arrived at the same value 4/3 for this crossover exponent. Moreover, since they argued that right at the critical point (the only case they considered) there is only one independent exponent, we have made contact with their entire analysis as regards exponents.

In summary we anticipate that near the critical point the mean square load will follow the scaling form [Eq. (78)]. Using simple arguments we have conjectured values for all the exponents [Eqs. (80), (81), and (84)] and guessed some features of the scaling function. As a check we have made contact with the critical point analysis of Majumdar and Sire and recovered the known value of the crossover exponent, 4/3 [28]. In the remainder of this section we will fully confirm the deductions we have made above. We will obtain an exact formula for the evolution of the mean square load; the exponents, θ, φ, μ, and κ; and the scaling function $\mathcal{C}$.

A. Disorder average and exact solution

As in Sec. II our strategy is to analyze the evolution of the correlation function $c_n(t)$; the mean-squared weight $\langle w^2(t) \rangle = c_0(t)$. The analysis is given in outline since most of the needed technical elements have already been described in Sec. II. Here we shall focus on the new complications introduced by consideration of injection.

Following the method of Sec. II B we first obtain the evolution equation for the correlation function, now including injection. Schematically this equation has the form

$$c_m(t+1) = \sum_n H_{mn} c_n(t) + \xi_m(t), \tag{88}$$

where H_{mn} is the same matrix as in Eq. (15). The effect of injection appears in the inhomogeneous term ξ_m. Explicitly

$$\xi_m = 2\langle I \rangle + (2t+1)\langle I \rangle^2 + \langle \delta I^2 \rangle \delta_{m=0}. \tag{89}$$

Our strategy to solve Eq. (88) is to first expand $c(t)$ and $\xi(t)$ in terms of the right eigenvectors of H,

$$c_m(t) = \sum_\lambda a_\lambda(t) \phi_m^\lambda; \quad \xi_m(t) = \sum_\lambda \xi_\lambda(t) \phi_m^\lambda. \tag{90}$$

As discussed before, the expansion amplitudes a_λ and ξ_λ are calculated by use of the left eigenvectors

$$a_\lambda(t) = \sum_m (\psi_m^\lambda)^* c_m(t); \quad \xi_\lambda(t) = \sum_m (\psi_m^\lambda)^* \xi_m(t). \tag{91}$$

In Sec. II B we have calculated the amplitudes for $c_m(t \to 0)$. We found $a^{(+)}(k, t \to 0) = a^{(-)}(k, t \to 0) \equiv a(k, t \to 0)$ with

$$a(k, t \to 0) = 2\pi \mathcal{A}(k)^* \delta(k) + [1 - \mathcal{A}(k)^*] i \cot \frac{k}{2}. \tag{92}$$

Here $\mathcal{A}(k)$ is given by Eq. (35). Similarly $\xi^{(+)}(k, t \to 0) = \xi^{(-)}(k, t \to 0) \equiv \xi(k, t \to 0)$ with

$$\xi(k,t) = \langle \delta I^2 \rangle \mathcal{A}(k)^* + \{2\langle I \rangle + (2t+1)\langle I \rangle^2\} \left\{ 2\pi \mathcal{A}(k)^* \delta(k) \right.$$
$$\left. + [1 - \mathcal{A}(k)^*] i \cot \frac{k}{2} \right\}. \tag{93}$$

Substituting the expansions Eq. (91) into the evolution Eq. (88) shows that the dynamics of the amplitudes for different right eigenvectors is decoupled and is given by

$$a_\lambda(t+1) = \lambda a_\lambda(t) + \xi_\lambda(t). \tag{94}$$

To solve this dynamics we introduce the z transforms

$$a_\lambda(z) = \sum_{t=0}^\infty a_\lambda(t) z^t,$$

$$\xi_\lambda(z) = \sum_{t=0}^\infty \xi_\lambda(t) z^t, \tag{95}$$

to obtain

$$a_\lambda(z) = \frac{a_\lambda(t\to 0)}{1-z\lambda} + \frac{z\xi_\lambda(z)}{1-z\lambda}. \tag{96}$$

Combining Eqs. (90) and (96) we conclude

$$c_m(z) = \sum_\lambda \left[\frac{a_\lambda(t\to 0)}{1-z\lambda} + \frac{z\xi_\lambda(z)}{1-z\lambda} \right] \phi_m^\lambda. \tag{97}$$

More explicitly

$$c_0(z) = 2 \int_0^\pi dk \frac{a(k,t\to 0)A(k)}{1-z\lambda(k)} + 2z \int_0^\pi dk \frac{\xi(k,z)A(k)}{1-z\lambda(k)}. \tag{98}$$

Here $c_0(z)$ is the z transform of $c_0(t)$; $A(k)$ is given by Eq. (30); $\lambda(k)$, by Eq. (29); and $a(k,t\to 0)$, by Eq. (92). $\xi(k,z)$ is to be obtained by z transforming Eq. (93).

Now all the pieces have been assembled. It remains to perform the k integral and invert the z transform. The k integrals may be performed by the standard contour integration method mentioned in footnote 2. The z transforms can all be inverted as illustrated in Appendix B.

After much calculation we find

$$\langle w^2(t) \rangle = \bar{F}(t,\epsilon) + \langle \delta I^2 \rangle M(t,\epsilon) + \langle I \rangle K(t,\epsilon) + \langle I \rangle^2 L(t,\epsilon) \tag{99}$$

with

$$\bar{F}(t,\epsilon) = \frac{\epsilon}{1-\epsilon} - \frac{1}{\pi\epsilon} \Gamma F_1,$$

$$M(t,\epsilon) = -\frac{\epsilon}{(1-\epsilon)^2} + \frac{2}{\pi} \frac{(1-\epsilon)}{\epsilon^2} \Gamma[tF_1 + F_2],$$

$$\tag{100}$$

$$K(t,\epsilon) = \frac{2}{1-\epsilon} t + \frac{2\epsilon^2}{(1-\epsilon)^3} - \frac{4}{\pi\epsilon} \Gamma[tF_1 + F_2],$$

$$L(t,\epsilon) = \frac{\epsilon^4 + 2\epsilon^3 - \epsilon^2}{(1-\epsilon)^5} + \frac{2\epsilon^2}{(1-\epsilon)^3} t + \frac{2}{3\pi\epsilon} \Gamma[(4t^2 - t)F_1$$
$$+ (8t-5)F_2 + 8F_3].$$

We have put an overline on $\bar{F}(t,\epsilon)$ to avoid confusion with a hypergeometric function. For brevity we have written

$$\Gamma = \frac{\Gamma(1/2)\Gamma(t+3/2)}{\Gamma(t+2)},$$

$$F_n = F\left(n, t+\frac{3}{2}, t+2; \frac{2\epsilon-1}{\epsilon^2}\right) \tag{101}$$

in Eq. (100).

Equations (100) is the final result of this section. It gives the evolution of load fluctuations for the q model with injection in $1+1$ dimensions. It holds for any distribution of fractions $P(f)$ and at any depth.
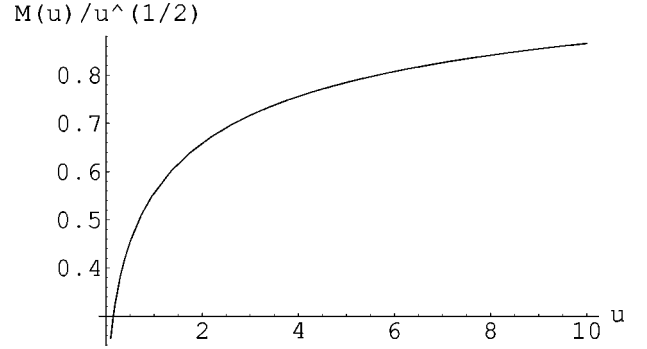

FIG. 5. Growth of load fluctuations with depth for the $1+1$ dimensional q-model close to the critical point. The scaling function $\mathcal{M}(u)$ gives the contribution due to fluctuations in the weight of beads [Eqs. (79) and (102)]. Here $\mathcal{M}(u)/\sqrt{u}$ is plotted as a function of u.

B. Scaling limit

More interesting than the exact results is the scaling behavior that emerges for $t \gg 1$ and $\delta = 1 - \epsilon \to 0$. To derive this behavior it is useful to express the hypergeometric functions in Eq. (100) via the integral representation, Eq. (45). The asymptotic behavior of ΓF_1 has been analyzed in Sec. II C [cf. Eqs. (47) and (48)]. The corresponding analysis of ΓF_2 and ΓF_3 is very similar and finally leads to

$$\bar{F}(t,\epsilon) \to \frac{1}{\delta} \left\{ 1 - \frac{2}{\pi} \Phi_1(u) \right\},$$

$$M(t,\epsilon) \to \frac{1}{\delta^2} \left\{ -1 + \frac{4}{\pi} u\Phi_1(u) + \frac{4}{\pi} \Phi_2(u) \right\},$$

$$\tag{102}$$

$$K(t,\epsilon) \to \frac{1}{\delta^3} \left\{ 2u+2 - \frac{8u}{\pi} \Phi_1(u) - \frac{8}{\pi} \Phi_2(u) \right\},$$

$$L(t,\epsilon) \to \frac{1}{\delta^5} \left\{ 2+2u+u^2 - \frac{16}{3\pi} [u^2\Phi_1(u) + 2u\Phi_2(u) + 2\Phi_3(u)] \right\}.$$

Here $u = t\delta^2$. For brevity we have written

$$\Phi_n(u) = \int_0^\infty ds \frac{e^{-us^2}}{(1+s^2)^n}. \tag{103}$$

Comparing Eqs. (79) to (102) we conclude that the exponents are $\theta = 1$, $\varphi = 2$, $\kappa = 1$, and $\mu = 1$ as conjectured. It is also straightforward to extract the scaling functions $\mathcal{F}(u)$, $\mathcal{M}(u)$, $\mathcal{K}(u)$, and $\mathcal{L}(u)$ from Eq. (102). The scaling functions are plotted in Figs. 4, 5, 6, and 7, respectively.

The asymptotics of the integrals $\Phi_n(u)$ are analyzed in Appendix C. Using those results we conclude that for small u
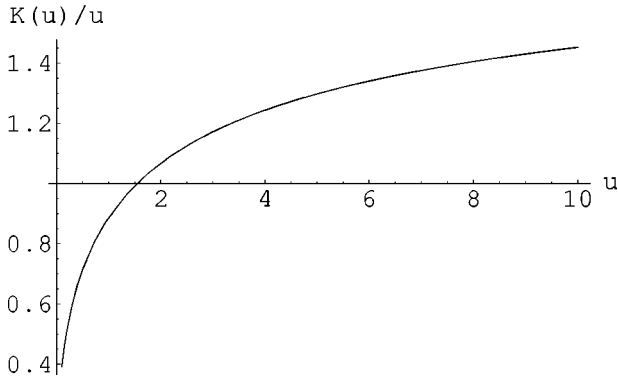
FIG. 6. Growth of load fluctuations with depth for the $1+1$ dimensional q model close to the critical point. The scaling function $\mathcal{K}(u)$ gives a contribution proportional to the average weight of beads [Eqs. (79) and (102)]. Here $\mathcal{K}(u)/u$ is plotted as a function of u.

$$\mathcal{F}(u) \approx \frac{2}{\sqrt{\pi}} u^{1/2},$$

$$\mathcal{M}(u) \approx u,$$

$$\mathcal{K}(u) \approx \frac{8}{3\sqrt{\pi}} u^{3/2}, \qquad (104)$$

$$\mathcal{L}(u) \approx \frac{16}{15\sqrt{\pi}} u^{5/2}.$$

For large u

$$\mathcal{F}(u) \approx 1,$$

$$\mathcal{M}(u) \approx \frac{2}{\sqrt{\pi}} \sqrt{u}, \qquad (105)$$
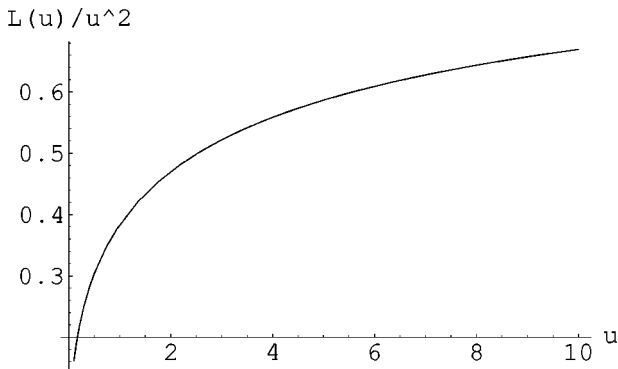
$$\mathcal{K}(u) \approx 2u,$$

FIG. 7. Growth of load fluctuations with depth for the $1+1$ dimensional q model close to the critical point. The scaling function $\mathcal{L}(u)$ gives a contribution proportional to the square of the average weight of beads [Eqs. (79) and (102)]. Here $\mathcal{L}(u)/u^2$ is plotted as a function of u.

$$\mathcal{L}(u) \approx u^2.$$

Substituting the small u asymptotics in Eq. (79) we obtain the behavior for depths small compared to $1/\delta^2$.

$$\langle w^2(t) \rangle \approx \frac{2}{\sqrt{\pi}} t^{1/2} + \langle \delta I^2 \rangle t + \langle I \rangle \frac{8}{3\sqrt{\pi}} t^{3/2} + \langle I \rangle^2 \frac{16}{15\sqrt{\pi}} t^{5/2}. \qquad (106)$$

This behavior would persist for all depths right at the critical point. Note that Eq. (106) agrees with the forms conjectured in Eqs. (82), (85), and (86) (including the numerical coefficient in the first case). It is hardly necessary to add that Eq. (106) is consistent with the critical point analysis of Majumdar and Sire since it leads, by the arguments given earlier in this section, to their crossover exponent 4/3 [28].

The large u asymptotics give the behavior at depths large compared to $1/\delta^2$. We find

$$\langle w^2(t) \rangle = \frac{1}{\delta} + \langle \delta I^2 \rangle \frac{1}{\delta} \frac{2}{\sqrt{\pi}} t^{1/2} + \langle I \rangle \frac{1}{\delta} 2t + \langle I \rangle^2 \frac{1}{\delta} t^2. \qquad (107)$$

The term proportional to $\langle I \rangle^2$ has the form anticipated in Eq. (87); at the greatest depths this term is dominant.

In summary we have shown that the singular distribution is an isolated critical point. Near the critical point the fluctuations in load have the scaling form Eq. (79). We have derived this scaling form and all the exponents. The results are in agreement with expectations based on simpler (non-rigorous) arguments.

V. HIGHER DIMENSIONS

We now turn to the q model in $D+1$ dimensions. The quantum Hall multilayer and river networks are both $1+1$ dimensional systems; bead packs however are described by the $2+1$ dimensional q model. The behavior of the model as a function of D is of intrinsic interest moreover. We will find that right at the critical point the growth exponents vary smoothly with dimension for $D<2$. Above $D=2$ they become fixed, revealing $D=2$ as the upper critical dimension for the critical case. Off the critical point we expect the fluctuations to grow according to a scaling function $\mathcal{F}(x)$ [Eq. (7)]. We will study how the function and exponents vary with dimensionality below $D=2$. For simplicity in this section we neglect injection.

A. Model and disorder average

First we must generalize the description of the q-model, so far confined to $1+1$ dimensions. The case of $2+1$ dimensions is easy to visualize. Figure 8 illustrates a square lattice composed of two interpenetrating square sublattices. The coordinates of sites $\vec{n} = (n_1, n_2)$ are both even for the black sites; both odd for the gray. The displacements from a site on either sublattice to its four nearest neighbors on the *other* sublattice are $(\pm 1, \pm 1)$. We will denote these displacements $\vec{u}$. In the q model planes of such square lattices are stacked
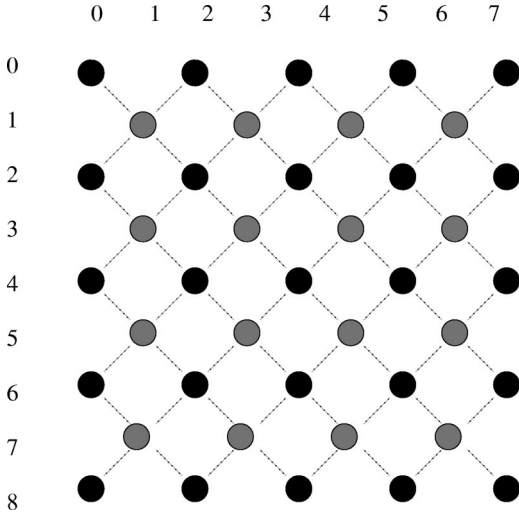
FIG. 8. Horizontal slice through the $2+1$ dimensional q model. Beads occupy the even (black) or odd (gray) sublattice in alternate layers. Each bead is supported by its four nearest neighbors in the layer below.

vertically. The beads alternately occupy only even or odd sublattices. Denoting the depth of a layer t, for t even only the even sublattice is occupied; for t odd, only the odd sublattice. Viewed in three dimensions the beads occupy a body-centered cubic structure. In the same sense, Fig. 1 can be viewed as a body-centered square structure.

Now consider a D dimensional simple cubic lattice. The co-ordinates of a site are specified by $\vec{n}=(n_1,n_2,\ldots,n_D)$ where n_i are integers. For the even sublattice the n_i are even; for the odd sublattice, they are odd. Each site has 2^D nearest neighbors on the other sublattice. We denote the displacements $(\pm 1,\pm 1,\ldots,\pm)$ to these neighbors $\vec{u}$. The $D+1$ dimensional q model consists of D dimensional cubic lattices stacked in the "vertical" t direction. In alternate t slices only the even or odd sublattices are occupied by beads.

It is assumed that a random fraction of the load on each bead is supported by its 2^D neighbors in the layer below. The fractions must sum to one;

$$\sum_{\vec{u}} f_{\vec{u}}=1. \tag{108}$$

Here $f_{\vec{u}}$ is the fraction of load transmitted by the bead to the neighbor separated by a horizontal displacement of $\vec{u}$. Hence the dynamics of the q model is governed by

$$w(\vec{n},t+1)=\sum_{\vec{u}} f_{\vec{u}}(\vec{n}-\vec{u},t)w(\vec{n}-\vec{u},t). \tag{109}$$

Equation (109) is the $D+1$ dimensional generalization of Eq. (1).

The fractions for a particular bead are assumed to be drawn from a distribution that is symmetric with respect to direction and respects the constraint Eq. (108). It follows

$$\langle f_{\vec{u}}\rangle=\frac{1}{2^D}. \tag{110}$$

We write

$$\langle f_{\vec{u}}^2\rangle=\frac{1}{2^{2D}}+\frac{\epsilon}{2^{2D}}, \tag{111}$$

where ϵ is a parameter that characterizes the distribution of fractions. From the sum constraint Eq. (108) it follows

$$\langle f_{\vec{u}_1} f_{\vec{u}_2}\rangle=\frac{1}{2^{2D}}-\frac{\epsilon}{(2^D-1)}\frac{1}{2^{2D}} \tag{112}$$

for $\vec{u}_1\neq\vec{u}_2$. The fractions are assumed to be independently and identically distributed for different beads.

For the singular distribution all the fractions are zero except one. The probability for each fraction to be one is $1/2^D$. It is easy to calculate $\epsilon=2^D-1$ for the singular distribution using Eq. (111) and to verify Eqs. (110) and (112) are satisfied. Since $\epsilon=2^D-1$ for the singular distribution we shall use δ, defined by

$$\delta=1-\frac{\epsilon}{(2^D-1)}, \tag{113}$$

as our measure of the distance of a distribution from the critical point.

As before it is useful to consider the correlation function

$$c(\vec{m},t)=\sum_{\vec{n}} \langle w(\vec{n},t)w(\vec{n}+\vec{m},t)\rangle. \tag{114}$$

Note that $\vec{m}$ is a D dimensional vector with even integer entries for both t even and t odd. The correlation function therefore lives on a simple cubic lattice in D dimensions. By rescaling, as in Sec. II A, we reduce the lattice constant of this lattice to one so that the components of the vector $\vec{m}$ are now integers. The variance in load is related to the on-site correlation by

$$\langle \delta w^2(t)\rangle=c(\vec{m}\rightarrow 0,t)-1. \tag{115}$$

Following the discussion of Sec. II A and using Eqs. (109), (110), (111), and (112) it is easy to show that the correlation function evolves with depth according to

$$c(\vec{m},t+1)=\frac{1}{2^D}c(\vec{m},t)+\frac{1}{2^{D+1}}\sum_{b=\text{nn}} c(\vec{m}+\vec{b},t) \tag{116}$$

$$+\frac{1}{2^{D+2}}\sum_{b=\text{nnn}} c(\vec{m}+\vec{b},t)+\cdots$$

$$+\frac{1}{2^{2D}}\sum_{\vec{b}=\text{n}\ldots\text{n}} c(\vec{m}+\vec{b},t)+\frac{\epsilon}{2^D}c(\vec{m},t)\delta_{\vec{m}=0}$$

$$-\frac{\epsilon}{(2^D-1)}\frac{1}{2^{D+1}}\sum_{b=\text{nn}}c(\vec{m}+\vec{b},t)\delta_{\vec{m}+\vec{b}=0}$$

$$-\frac{\epsilon}{(2^D-1)}\frac{1}{2^{D+2}}\sum_{b=\text{nnn}}c(\vec{m}+\vec{b},t)\delta_{\vec{m}+\vec{b}=0}\cdots$$

$$-\frac{\epsilon}{(2^D-1)}\frac{1}{2^{2D}}\sum_{b=\text{n}\ldots\text{n}}c(\vec{m}+\vec{b},t)\delta_{\vec{m}+\vec{b}=0}.$$

While reading Eq. (116) it is useful to recall that the correlation function lives on a D dimensional cubic lattice. For $D=2$ each site has four nearest neighbors and four next-nearest neighbors. For general D, each site has $2D$ nearest neighbors; $2^2C(D,2)$ next nearest neighbors; $2^3C(D,3)$ third nearest neighbors; and $2^DC(D,D)$ Dth nearest neighbors. In Eq. (116) $\vec{b}$ denotes the displacement from a site to any of these neighbors; nn denotes nearest neighbor; nnn, next nearest; and so forth.

In the next section we will solve Eq. (116) for $c(\vec{m}\to 0,t)$ subject to the initial condition that a uniform load has been applied to the top layer. Thus $c(\vec{m},t\to 0)=1$ for all $\vec{m}$.

B. Solution

It is easy to verify that

$$c(\vec{m},t\to\infty)=\begin{cases}\dfrac{1}{\delta} & \text{for } \vec{m}=0 \\ 1 & \text{otherwise}\end{cases} \tag{117}$$

is a steady state solution to Eq. (116). Equation (117) shows that the variance $\langle\delta w^2\rangle$ saturates at sufficient depth in all dimensions for all distributions except the singular.

We now calculate the evolution of the variance with depth using a method different from that of Sec. II [30]. First we z transform the (discrete) t dependence of the correlation function,

$$c(\vec{m},z)=\sum_{t=0}^{\infty}c(\vec{m},t)z^t, \tag{118}$$

and Fourier transform the space dependence,

$$c(\vec{p},z)=\sum_m e^{-i\vec{p}\cdot\vec{m}}c(\vec{m},z). \tag{119}$$

The use of the same symbol for the correlation and its transforms, although customary, is potentially confusing. For example, $c(\vec{p},t\to 0)$ denotes the Fourier transform of $c(\vec{m},t)$ at $t=0$; no z transform is implied.

Performing both transforms on Eq. (116) we obtain

$$c(\vec{p},z)=c(\vec{p},t\to 0)+zc(\vec{p},z)S(\vec{p})+\frac{\epsilon}{2^D-1}zc(\vec{m}\to 0,z). \tag{120}$$

Here

$$S(\vec{p})=\frac{1}{2^D}\left\{1+\frac{1}{2}\sum_{b=\text{nn}}e^{i\vec{p}\cdot\vec{b}}+\frac{1}{2^2}\sum_{b=\text{nnn}}e^{i\vec{p}\cdot\vec{b}}+\cdots\right.$$

$$\left.+\frac{1}{2^D}\sum_{b=\text{n}\ldots\text{n}}e^{i\vec{p}\cdot\vec{b}}\right\}$$

$$=\frac{(1+\cos p_1)}{2}\frac{(1+\cos p_2)}{2}\cdots\frac{(1+\cos p_D)}{2} \tag{121}$$

is a "structure factor" for the cubic lattice. It will also prove convenient to define

$$G(\vec{p},z)=\frac{1}{1-zS(\vec{p})}. \tag{122}$$

Both $S(\vec{p})$ and $G(\vec{p},z)$ have helpful physical interpretations that we shall make use of below. For the moment we rearrange Eq. (120) to obtain

$$c(\vec{p},z)=c(\vec{p},t\to 0)G(\vec{p},z)$$
$$+(1-\delta)zc(\vec{m}\to 0,z)[1-S(\vec{p})]G(\vec{p},z). \tag{123}$$

By inverting the Fourier transform we can turn Eq. (123) into an expression for $c(\vec{m}\to 0,z)$. After further rearrangement

$$c(\vec{m}\to 0,z)=\frac{\displaystyle\int\frac{d\vec{p}}{(2\pi)^D}c(\vec{p},t\to 0)G(\vec{p},z)}{1-(1-\delta)z\displaystyle\int\frac{d\vec{p}}{(2\pi)^D}[1-S(\vec{p})]G(\vec{p},z)}. \tag{124}$$

Equation (124) is a general expression for $c(\vec{m}\to 0,z)$ for an arbitrary initial condition. For uniform loading of the top layer

$$c(\vec{p},t\to 0)=(2\pi)^D\delta(\vec{p}). \tag{125}$$

It follows from Eqs. (121) and (122) that $G(\vec{p}\to 0,z)=1/(1-z)$; hence Eq. (124) simplifies to

$$c(\vec{m}\to 0,z)=(1-z)^{-1}\left\{1-(1-\delta)z\int\frac{d\vec{p}}{(2\pi)^D}\right.$$

$$\left.\times[1-S(\vec{p})]G(\vec{p},z)\right\}^{-1}. \tag{126}$$

Equation (126), together with the definitions of the structure factor [Eq. (121)] and $G(\vec{p},z)$ [Eq. (122)], constitutes an exact formal evaluation of the variance with depth. To obtain $\langle\delta w^2(t)\rangle$ explicitly it only remains to perform the integral over $\vec{p}$ and to invert the z transform. We return to this task in the next section. We conclude this section with a useful interpretation of $S(\vec{p})$ and $G(\vec{p},z)$.

Equation (116) with $\epsilon \to 0$ resembles the Schrödinger equation for a particle on a D dimensional cubic lattice with hopping to the nearest neighbors, the next nearest neighbors, and so on to the Dth nearest neighbors. It is not difficult to see that the eigenstates of this Schrödinger equation are plane waves. $S(\vec{p})$ is the dispersion relation, the eigenvalue at wave vector $\vec{p}$. From Eq. (121) we see that the energy level spectrum is a continuous band between zero and one.

The momentum space Green's function for this tight-binding lattice would normally be written

$$\mathcal{G}(\vec{p},E) = \frac{1}{E - S(\vec{p})}. \qquad (127)$$

Comparing Eq. (127) to Eq. (122) we see that $G(\vec{p},z)$ is essentially the Green's function with $E \to 1/z$. It is familiar from quantum mechanics that the real space Green's function at the origin,

$$\mathcal{G}(\vec{m} \to 0,E) = \int \frac{d\vec{p}}{(2\pi)^D} \frac{1}{E - S(\vec{p})}, \qquad (128)$$

regarded as a function of (complex) E, has a branch cut running from $E=0$ to $E=1$, the interval that supports the eigenvalue band. It is not difficult to use the familiar arguments to conclude that, regarded as a function of complex z, $c(\vec{m} \to 0,z)$ has a branch cut along the line $z=1$ to ∞ (onto which the segment $[0,1]$ maps under the transformation $E \to 1/z$). The analytic properties of $c(\vec{m} \to 0,z)$ will prove useful in the next section.

C. Scaling limit

In this section we study the evolution of the variance in the large depth scaling limit. Thus $t \gg 1$ and δ is zero or very close to it throughout.

An advantage of studying the large depth limit is that we do not have to calculate $c(\vec{m} \to 0,z)$ exactly; it is only necessary to calculate the leading behavior as $z \to 1$. One way to understand this is to consider the critical case $\delta = 0$. In this case we expect that at great depth

$$c(\vec{m} \to 0,t) \sim t^x. \qquad (129)$$

It is easy to show that for $f(t) = t^x$, the z transform is $\Gamma(x+1)/(1-z)^{x+1}$ plus less singular terms. Thus for a function that behaves as t^x for large t also the z transform is

$$t^x \leftrightarrow \frac{\Gamma(x+1)}{(1-z)^{x+1}} + (\text{less singular}). \qquad (130)$$

If we know the leading singularity of $c(\vec{m} \to 0,z)$ as $z \to 1$ we can use Eq. (130) to read off the large depth behavior.

Another way to see that we only need the behavior of $c(\vec{m} \to 0,z)$ as $z \to 1$ is to consider inverting the z transform by the contour integral method of Appendix B. This is accomplished by folding the contour over the branch point of

$c(\vec{m} \to 0,z)$ at $z=1$ and integrating along the cut. In that integral $c(\vec{m} \to 0,z)$ is weighted by a factor that decays extremely rapidly away from $z=1$ at large depths.

Our goal therefore is to analyze the $z \to 1$ behavior of

$$G(z) = \int \frac{d\vec{p}}{(2\pi)^D} \frac{1}{1 - zS(\vec{p})}, \qquad (131)$$

since by a straightforward rearrangement the integral in Eq. (126) simplifies to

$$\int \frac{d\vec{p}}{(2\pi)^D} [1 - S(\vec{p})] G(\vec{p},z) = \left(1 - \frac{1}{z}\right) G(z) + \frac{1}{z}. \qquad (132)$$

Insight into the behavior of $G(z)$ can be gained by expanding $S(\vec{p})$ around $\vec{p} = 0$ to obtain

$$G(z) \approx \int \frac{d\vec{p}}{(2\pi)^D} \frac{1}{(1-z) + \vec{p}^2/4}. \qquad (133)$$

If we set $z=1$ in Eq. (133) the integrand diverges as $\vec{p} \to 0$ for $D \leq 2$; it is regular in more than two dimensions. Thus in more than two dimensions $G(z)$ has a branch point at $z=1$ but there is no actual divergence. In two dimensions or less there is an actual divergence.

The leading behavior of $G(z)$ above two dimensions is thus simply obtained by setting $z=1$ in Eq. (131):

$$G(z) \approx G(1) \quad \text{for } D > 2. \qquad (134)$$

In two dimensions we can obtain the singularity by recognizing $G(z)$ to be a Jacobi elliptic integral. Square lattice Green's functions are known to be related to Jacobi's elliptic functions; but since our lattice features next-nearest neighbor hopping, in addition to the customary nearest neighbor hopping, we outline the analysis in Appendix D. The result is that for $z \to 1$

$$G(z) \approx -\frac{1}{\pi} \ln(1-z) \quad \text{for } D = 2. \qquad (135)$$

For $D < 2$ we obtain the singular behavior of $G(z)$ in Appendix D. The result is

$$G(z) = \frac{\Gamma(1 - D/2)}{\sqrt{\pi^D}} (1-z)^{D/2 - 1} \quad \text{for } D < 2. \qquad (136)$$

An important feature revealed by this calculation is that the singular behavior of $G(z)$ is controlled by the long wavelength behavior of $G(p,z)$ for all $D < 2$; it breaks down as $D \to 2$. Although it is instructive to do the calculation for continuous D to examine the $D \to 2$ limit, the only case that is physically relevant is of course the integer dimension $D = 1$.

Equipped with the leading behavior of $G(z)$ in all dimensions we now obtain the long time behavior of $\langle \delta w^2(t) \rangle$. At the critical point we set $\delta = 0$ and substitute Eqs. (132),

(134), (135), and (136) in Eq. (126). Except in two dimensions the z transforms may be inverted by inspection of Eq. (130). For two dimensions we must resort to the method of Appendix B and finally obtain

$$\langle \delta w^2(t) \rangle = \pi^{D/2-1} \sin\left(\frac{\pi D}{2}\right) t^{D/2} \quad \text{for } D < 2$$

$$= \frac{t}{\ln t} \quad \text{for } D = 2$$

$$= \frac{1}{G(1)} t \quad \text{for } D > 2. \tag{137}$$

As indicated by the simple steady state solution, at the critical point the fluctuations grow without bound as a power of t for all dimensions. The exponent becomes independent of D for $D > 2$ revealing $D = 2$ as the upper critical dimension.

By substituting Eqs. (132) and (136) in Eq. (126) we can also obtain the behavior of $\langle \delta w^2(t) \rangle$ away from the critical point for less than two dimensions. Inverting the z transform by the method of Appendix B we find

$$\langle \delta w^2(t) \rangle = \frac{1}{\delta^\theta} \mathcal{F}(t \delta^\varphi). \tag{138}$$

Here the exponents

$$\theta = 1, \quad \varphi = \frac{2}{D} \tag{139}$$

and the scaling function

$$\mathcal{F}(u) = \frac{1}{D} - \frac{2}{\pi D} \int_0^\infty ds \, \frac{1}{1+s^2} \exp - \frac{u s^{2/D}}{q_D^{2/D}} \tag{140}$$

with $q_D = \Gamma(1 - D/2) \sin(\pi D/2) / \sqrt{\pi}^D$ a dimension dependent constant. Again, only the result for $D = 1$ is physically meaningful; in this case Eq. (140) coincides with the result of Sec. II.

In summary the main results of this section are that for all distributions, except the singular, at sufficient depth the load fluctuations saturate and (in agreement with experiment) there are no horizontal correlations in load [Eq. (117)]. The saturation value of the load variance diverges as the critical point is approached. At the critical point the load fluctuations grow without bound as a power of depth [Eq. (137)]. Below two dimensions this exponent depends on dimensionality; above two dimensions it is constant, revealing $D = 2$ as the critical dimension. At the critical dimension the growth of fluctuations is tempered by a logarithmic factor as might be expected at a critical dimension. We have also evaluated the scaling function that describes the growth and saturation of load fluctuations near the critical point for $D < 2$.
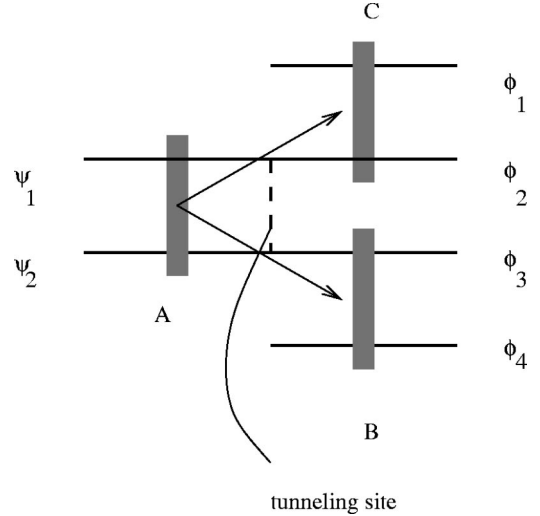

FIG. 9. Elementary vertex of the Saul, Kardar, and Read model.

VI. QUANTUM HALL MULTILAYER

A. Models

In this section we turn to the chiral wave models that are believed to adequately describe the surface electronic states of a quantum Hall multilayer. We begin by examining the circumstances under which the quantum network model of Saul, Kardar, and Read [6] discussed in Sec. I is equivalent to a q model.

Following Saul, Kardar, and Read, the first step is to identify pairs of links (joined by vertical gray bars in Fig. 9) as "beads." The "load" on a bead is the total probability that the electron is on either of its two constituent links. Load propagates from left to right now rather than top to bottom as it did in our earlier depictions of the q model. For this reason we will label the vertical co-ordinate n and the horizontal co-ordinate t here (see Fig. 3).

To analyze how load propagates consider an elementary vertex of the Saul, Kardar, and Read model shown in Fig. 9. The wave function amplitudes are related via

$$\begin{pmatrix} \phi_2 \\ \phi_3 \end{pmatrix} = S \begin{pmatrix} \psi_1 \\ \psi_2 \end{pmatrix}; \tag{141}$$

here S is a random 2×2 su(2) rotation matrix. Saul, Kardar, and Read assumed the S matrices were drawn from the invariant distribution for the su(2) group [31]. The loads on beads A, B, and C are, respectively, $|\psi_1|^2 + |\psi_2|^2$, $|\phi_1|^2 + |\phi_2|^2$ and $|\phi_3|^2 + |\phi_4|^2$. By unitarity $|\psi_1|^2 + |\psi_2|^2 = |\phi_3|^2 + |\phi_4|^2$. Thus bead A sends a fraction f of its load to neighbor B and the remainder $1 - f$ to neighbor C.

A key feature of the Saul, Kardar, and Read model is that the distribution of the fractions, $P(f)$ is independent of the input amplitudes ψ_1 and ψ_2. This follows from the assumed group invariant distribution for the S matrices. It is this feature that allows the Saul, Kardar, and Read model to be mapped onto a q model.

To derive the distribution of the fractions recall that an su(2) matrix may be parametrized $S = x_0 + i\vec{x} \cdot \vec{\sigma}$ with $(x_0, \vec{x})$

real and subject to $x_0^2 + \vec{x}^2 = 1$. If we take $\psi_1 = 1, \psi_2 = 0$ then $f = x_0^2 + x_1^2$. From the invariant distribution for su(2) matrices,

$$P(x_0, \vec{x}) = \frac{1}{\pi} \delta(x_0^2 + \vec{x}^2 - 1), \qquad (142)$$

it is not difficult to show that the fraction f follows the uniform distribution, $P(f) = 1$ for $0 < f < 1$.

Now suppose the wave function is known through the vertical slice $t = 0$. We could propagate the wave function t slices to the right using the quantum Saul, Kardar, and Read model. Alternatively we could calculate the load in the initial layer and propagate it to the right using the q model with uniform distribution. Either way the load we obtain in layer t would be the same statistically. This is the sense in which the Saul, Kardar, and Read model is equivalent to the q model.

Note that the q model does not keep track of phase information. The mapping is useful only under circumstances that the phase information is unimportant. Below we will discuss some problems of wave packet dynamics for which the mapping is useful. The mapping can also be used to study vertical transport in the quantum Hall multilayer in the limit of large circumference but we do not discuss that application here.

An obvious circumstance when the phase information is important and the mapping cannot be used is if periodic boundary conditions are imposed in the horizontal t direction, as would be appropriate for a multilayer in the fully phase-coherent, mesoscopic regime. Phase information is needed to match the wave function after it is propagated around the circumference. We will develop this point in a more technical way in Sec. VI C.

Another case in which a quantum network model will map onto a q model is if the wave functions and S matrices are chosen to be real and the S matrices are further assumed to be distributed over the subgroup of rotations about the y axis with appropriate invariant measure. The fraction distribution $P(f) = (1/\pi) f^{-1/2} (1-f)^{-1/2}$ for the q model that results. For most distributions of the S matrix however it is not possible to obtain even the limited mapping between the quantum network model and the classical q model obtainable in this and in the Saul, Kardar, and Read case.

Finally we present a convenient continuum model of the multilayer surface governed by the Schrödinger equation

$$-i \frac{\partial}{\partial t} \psi_n(t) = m_n(t) \psi_{n+1}(t) + m_{n-1}^*(t) \psi_{n-1}(t). \qquad (143)$$

Since the equation is first order in t, given the wave function at a fixed t slice we can use it to propagate the wave function to the right, just as in the discrete network model. In the transverse direction the model is discrete and second order. Disorder is incorporated by taking the hopping elements $m_n(t)$ to be random. For a discussion of the relationship between onsite and hopping disorder see Refs. [24,26]. Evidently this model cannot be reduced to a classical q model.

B. Wave-packet dynamics

In this section we briefly discuss wave-packet dynamics for the models of the previous section. Mathematically this problem is identical to the motion of a wave packet in a crystal with noise (temporal randomness). It also bears formal resemblance to the directed polymer model, an important problem in statistical mechanics. Hence it is a problem of general interest and has been studied since at least the 1970s from various points of view (see Ref. [6] and references therein). A considerable amount is now known.

For the Saul, Kardar, and Read model wave-packet dynamics can be studied using the mapping to the q model; indeed the mapping was introduced for this purpose. In this section we will formulate the problem and summarize known results. These results reveal that the q model and the continuum wave model introduced in the last section behave in qualitatively similar ways.

Consider an electron localized at $n = 0$ at $t = 0$. This wave packet can be propagated to the right using Eq. (143). As it propagates it will broaden and its mean position will deflect. It is interesting to know how the breadth and deflection grow with displacement and to analyze the distribution of "load" at sufficiently great displacement that a steady state is reached.

The root mean square width of the wave packet grows as the square root of the displacement. This was derived for the continuum model in the 1970s [32] and it is easy to show that the same form is obtained in the Saul, Kardar, and Read model. The root mean square deflection grows as the fourth root of the displacement. This result has been obtained numerically and analytically for both the Saul, Kardar, and Read [6,30,34] and continuum models [33,24].

To compare the distribution of load, for the continuum model we define the load on an edge as $w_n(t) = |\psi_n(t)|^2$. The asymptotic distribution of load, $\Pi(w, t \to \infty)$ was obtained by Coppersmith *et al.* for the q model [4]. For various distributions of the fractions, $P(f)$, they found that $\Pi(w, t \to \infty)$ decayed exponentially with w with a power law prefactor that depended on the distribution $P(f)$. For the uniform distribution the prefactor was a constant. The corresponding result for the continuum wave model was obtained by Ref. [25] by mapping the problem onto an su(1,1) quantum ferromagnet. Here too the result for the load distribution is an exponential with a prefactor linear in w.

C. Field theory formulation

We have emphasized above that the equivalence between the Saul, Kardar, and Read model and the q model is useful only when open boundary conditions are imposed in the horizontal t direction; it breaks down for periodic boundary conditions needed to describe transport in phase-coherent multilayers. The importance of boundary conditions is also reflected in field theory formulations of these models. In Ref. [24] the continuum model with open boundary conditions was mapped onto a Heisenberg ferromagnet. In contrast, with periodic boundary conditions a mapping to a supersymmetric analogue of the Heisenberg ferromagnet was obtained in Refs. [23,26].

In this section we derive the supersymmetric spin representation following the operator methods of Ref. [24]. This derivation highlights the role of boundary conditions, the feature we wish to emphasize here. It only makes use of operator methods and is in this sense more elementary than the functional methods of Ref. [26]. Moreover mappings to supersymmetric spin models have recently been used fruitfully not only to study the multilayer but also to provide nonperturbative insights into various other problems of electron localization [35–37]. It is hoped that the present derivation, with its emphasis on boundary conditions[4] and its use of operator methods will prove of interest in this broader context also.

1. Fermion representation

We wish to evaluate $G(n,t;n',t')$, the Green's function for the continuum model governed by the Schrödinger equation,

$$-i\frac{\partial}{\partial t}G(n,t;n',t')=m_n(t)G(n+1,t;n',t')$$

$$+m^*_{n-1}(t)G(n-1,t;n',t')$$

$$-i\delta(t-t')\delta_{nn'}, \qquad (144)$$

and subject to the periodic boundary condition

$$G(n,t+T;n',t')=G(n,t;n',t'). \qquad (145)$$

Here T is the period in the t direction. In Ref. [24], the Green's function was calculated subject to the chiral boundary condition, $G(n,t;n',t')=0$ for $t<t'$, leading to a simpler field theory formulation.

The key idea is to reinterpret the co-ordinate t as time. Equation (144) then describes a particle on a one-dimensional lattice with noise. In second quantized notation the (time-dependent) Hamiltonian that governs the motion of this fictitious particle is

$$H^R_F(t)=\sum_n [m_n(t)c^{R\dagger}_n c^R_{n+1}+m^*_{n-1}(t)c^{R\dagger}_n c^R_{n-1}].$$

$$(146)$$

Here $c^{R\dagger}_n$ creates a Fermion at site n; c^R_n annihilates it. The reasons for the superscript on the Fermion Hamiltonian and on the creation and annihilation operators will become apparent shortly.

The S matrix for this model obeys

$$-i\frac{\partial}{\partial t}S^R_F(t)=H^R_F(t)S^R_F(t) \qquad (147)$$

----

[4] For the effect of boundary conditions on the supersymmetry mapping for models such as the Chalker model of the quantum Hall transition see Refs. [36] and [37] where the random hopping model in one dimension is analyzed with periodic and open (scattering) boundary conditions, respectively.

subject to $S^R_F(t\to 0)=1$. From $S^{R-1}_F S^R_F=1$ it is easy to verify the useful result

$$i\frac{\partial}{\partial t}S^{R-1}_F=S^{R-1}_F(t)H^R_F(t). \qquad (148)$$

We define

$$c^R_n(t)=S^{R-1}_F(t)c_n S^R_F(t) \qquad (149)$$

and similarly for $c^{R\dagger}_n(t)$.

Now by analogy with finite temperature field theory [38] we write the Green's function

$$G(n,t;n',t')=\mathrm{Tr}[S^R_F(T)c^R_n(t)c^{R\dagger}_{n'}(t')]/Z^R_F(T) \quad \text{for } t>t'$$

$$=-\mathrm{Tr}[S^R_F(T)c^{R\dagger}_{n'}(t')c^R_n(t)]/Z^R_F(T)$$

$$\text{for } t<t',$$

$$Z^R_F(T)=\mathrm{Tr}[S^R_F(T)]. \qquad (150)$$

$Z^R_F(T)$ is analogous to the partition function in finite temperature field theory. It is easy to verify that G obeys the differential Eq. (144) by making use of Eqs. (147) and (148) and the commutation relation

$$[H^R_F(t),c^R_n]=-m_n(t)c^R_{n+1}-m^*_{n-1}(t)c^R_{n-1}. \qquad (151)$$

However,

$$G(n,T;n',t')=\mathrm{Tr}[S^R_F(T)S^{R-1}_F(T)c^R_n S^R_F(T)c^{R\dagger}_{n'}(t')]/Z^R_F(T)$$

$$=\mathrm{Tr}[S^R_F(T)c^{R\dagger}_{n'}(t')c^R_n]/Z^R_F(T)$$

$$=-G(n,0;n',t'). \qquad (152)$$

Thus G obeys antiperiodic rather than periodic boundary conditions. This problem is fixed by adding a term to the Hamiltonian

$$H^R_F(t)\to H^R_F(t)+\frac{\pi}{T}\sum_n c^{R\dagger}_n c^R_n. \qquad (153)$$

Alternatively we may replace $\mathrm{Tr}\to S\,\mathrm{Tr}$ in Eq. (150). By $S\,\mathrm{Tr}$ we mean the trace of an operator over all states with an even number of fermions minus the trace over states with an odd number of fermions.

We also need an expression for the complex conjugate of the Green's function since our ultimate purpose is to calculate the disorder average of $|G(n,t;n',t')|^2$, the diffusion propagator. To this end we complex conjugate Eq. (144) to obtain the differential equation obeyed by G^*. Comparison to Eq. (144) reveals that we should consider A fermions governed by the Hamiltonian

$$H^A_F(t)=-\sum_n [m_n(t)c^{A\dagger}_{n+1}c^A_n+m^*_n(t)c^{A\dagger}_n c^A_n]. \qquad (154)$$

$G^*(n,t;n',t')$ is then given by the right hand side of Eq. (150) if we replace $R\to A$ and $\mathrm{Tr}\to S\,\mathrm{Tr}$.

As might be expected the Hamiltonian for the A fermions is related to that for the R fermions via a particle hole transformation. This symmetry between the R fermions and the A holes leads to an su(2) symmetry in the fermion sector of the complete field theory formulation that we obtain below [Eq. (171)]. It is also at the root of the supersymmetry of the field theory formulation.

In summary the Green's function with periodic boundary conditions may be generated from the second quantized Hamiltonian, $H_F^R(t)$ [Eqs. (153) and (146)] using the definition Eq. (150). The complex conjugate of the Green's function may be obtained similarly using the Hamiltonian $H_F^A(t)$ [Eq. (154)]. Equation (150) and its A fermion analogue provide exact formal expressions for the Green's function for a particular realization of the random tunneling $m_n(t)$. These expressions are not particularly convenient to average since $m_n(t)$ appears in both numerator and denominator.

2. Boson representation

Alternatively we could interpret Eq. (144) as a time dependent Schrödinger equation for bosonic particles on a one-dimensional lattice. The corresponding "time"-dependent bosonic Hamiltonian in second quantized notation is

$$H_B^R(t) = \sum_n [m_n(t)b_n^{R\dagger}b_{n+1}^R + m_{n-1}^*(t)b_n^{R\dagger}b_{n-1}^R].$$
(155)

Here $b_n^{R\dagger}$ creates an R boson at site n; b_n^R annihilates it.

The Green's function is now defined as

$$G(n,t;n',t') = \mathrm{Tr}[S_B^R(T)b_n^R(t)b_{n'}^{R\dagger}(t')]/Z_B^R(T) \quad \text{for } t>t'$$

$$= \mathrm{Tr}[S_B^R(T)b_{n'}^{R\dagger}(t')b_n^R(t)]/Z_B^R(T)$$

$$\text{for } t<t',$$

$$Z_B^R(T) = \mathrm{Tr}\, S_B^R(T).$$
(156)

Here S_B^R is the bosonic S matrix and $Z_B^R(T)$ is the bosonic analog of the partition function.

For greater rigor we must regulate the traces to ensure convergence but for brevity we do not discuss this explicitly here.

The complex conjugate of the Green's function is generated similarly if instead of the R bosons we consider A bosons governed by

$$H_B^A(t) = -\sum_n [m_n(t)b_{n+1}^{A\dagger}b_n^A + m_n^*(t)b_n^{A\dagger}b_{n+1}^A].$$
(157)

The main result of this subsection is Eq. (156). It provides a formal bosonic expression for the exact Green's function for a particular realization of random tunneling, $m_n(t)$. A similar expression for G^* may be obtained by working with the Hamiltonian Eq. (157). Like their fermionic counterparts these bosonic expressions are not particularly well suited for averaging over disorder.

3. Supersymmetry

We now develop an expression for the diffusion suitable for averaging over disorder. In Appendix E it is shown that

$$Z_F^R(T)Z_B^R(T) = 1.$$
(158)

Thus we consider a model that includes both A and R fermions and bosons governed by the Hamiltonian

$$H_{\mathrm{SUSY}}(t) = H_F^R(t) + H_F^A(t) + H_B^R(t) + H_B^A(t)$$

$$= \sum_n [m_n(t)A_n + m_n^*(t)A_n^\dagger].$$
(159)

Here

$$A_n = c_n^{R\dagger}c_{n+1}^R - c_{n+1}^{A\dagger}c_n^A + b_n^{R\dagger}b_{n+1}^R - b_{n+1}^{A\dagger}b_n^A.$$
(160)

The corresponding S matrix obeys

$$-i\frac{\partial}{\partial t}S_{\mathrm{SUSY}}(t) = H_{\mathrm{SUSY}}(t)S_{\mathrm{SUSY}}(t)$$
(161)

subject to $S_{\mathrm{SUSY}}(t\to0) = 1$. A formal solution to Eq. (161) is given by

$$S_{\mathrm{SUSY}}(t) = P\exp\left[i\int_0^t dt_1\, H_{\mathrm{SUSY}}(t_1)\right].$$
(162)

Here P is the chronological ordering operator.

Hence the diffusion is given by

$$|G(n,t;n',t')|^2 = S\,\mathrm{Tr}[S_{\mathrm{SUSY}}(T)c_n^R(t)c_n^A(t)c_{n'}^{A\dagger}(t')c_{n'}^{R\dagger}(t')]$$

$$\text{for } t>t'$$

$$= S\,\mathrm{Tr}[S_{\mathrm{SUSY}}(T)c_{n'}^{A\dagger}(t')c_{n'}^{R\dagger}(t')c_n^R(t)c_n^A(t)]$$

$$\text{for } t<t'. \quad (163)$$

The content of Eq. (163) is that to calculate the diffusion we must create or annihilate a pair of R and A fermions (depending on the time order). Then we must propagate this state in accordance with H_{SUSY} and perform an S matrix weighted trace. The Hamiltonian H_{SUSY} is noninteracting but it is random and time dependent.

Equation (163) is an exact formal expression for the diffusion. Note the lack of a denominator, eliminated by virtue of Eq. (158). This feature allows us to perform the average over disorder easily. For example,

$$\langle S_{\mathrm{SUSY}}(t)\rangle = \exp[-\mathcal{H}_{\mathrm{SUSY}}t]$$
(164)

with

$$\mathcal{H}_{\mathrm{SUSY}} = \frac{D}{2}\sum_n (A_n^\dagger A_n + A_n A_n^\dagger).$$
(165)

Here we have assumed that the tunneling $m_n(t)$ is a Gaussian white noise process with zero mean and variance

$$\langle m_n^{(\alpha)}(t) m_{n'}^{(\beta)}(t') \rangle = D\,\delta(t-t')\,\delta_{nn'}\,\delta_{\alpha\beta}. \qquad (166)$$

Here $m_n^{(1)}(t) = $ real part of $m_n(t)$; $m_n^{(2)}(t) = $ imaginary part of $m_n(t)$.

Recall that for a single Gaussian random variable y, the phase average $\langle e^{iy} \rangle = e^{-\langle y^2 \rangle/2}$. Equation (164) is analogous to this result but with the added complications that S_{SUSY} is an ordered exponential, not a simple exponential, and the average is over a random process rather than a single random variable. To derive Eq. (165) it is simplest to expand the time ordered exponential [Eq. (162)] and average term by term.

Proceeding in this manner we obtain an expression for the average diffusion

$$\langle |G(n,t;n',t')|^2 \rangle = S\,\mathrm{Tr}\{\exp[-\mathcal{H}_{\mathrm{SUSY}}(T-t+t')]c_n^R c_n^A$$
$$\times \exp[-\mathcal{H}_{\mathrm{SUSY}}(t-t')c_n^{A\dagger} c_n^{R\dagger}\}$$

$$\text{for } t > t'. \quad (167)$$

A similar expression may be written for the case $t < t'$. The content of Eq. (167) is that to calculate the *average* diffusion we must create (or for the other time order, annihilate) a pair of R and A fermions and propagate the resulting state according to the effective Hamiltonian $\mathcal{H}_{\mathrm{SUSY}}$. In contrast to H_{SUSY} the effective Hamiltonian is not time dependent or random but it is interacting.

This completes our formulation of the continuum directed wave model of Sec. VI A as a superspin field theory. The main results are the superspin Hamiltonian [Eq. (165)] and Eq. (167) that shows how interesting correlation functions are calculated in the superspin formulation. The usefulness of this formulation depends on the extent to which the superspin model can be analyzed.

In the remainder of this section we discuss the form and symmetry of the superspin Hamiltonian [Eq. (165)]. To this end it is helpful to introduce special notation for the boson and fermion bilinears of which $\mathcal{H}_{\mathrm{SUSY}}$ is composed. We denote the fermion bilinears

$$J_+ = c^{R\dagger} c^{A\dagger} = J_x + iJ_y,$$

$$J_- = c^A c^R = J_x - iJ_y,$$

$$\qquad (168)$$

$$J_z = \frac{1}{2}(c^{R\dagger} c^R + c^{A\dagger} c^A - 1),$$

$$J = \frac{1}{2}(c^{R\dagger} c^R - c^{A\dagger} c^A + 1);$$

the boson bilinears,

$$K_+ = b^{R\dagger} b^{A\dagger} = K_x + iK_y,$$

$$K_- = b^A b^R = K_x - iK_y,$$

$$\qquad (169)$$

$$K_z = \frac{1}{2}(b^{R\dagger} b^R + b^{A\dagger} b^A + 1),$$

$$K = \frac{1}{2}(b^{R\dagger} b^R - b^{A\dagger} b^A - 1);$$

and the mixed bilinears,

$$M_1 = b^{R\dagger} c^R, \quad M_2 = b^{A\dagger} c^A,$$

$$L_1 = b^{A\dagger} c^{R\dagger}, \quad L_2 = b^{R\dagger} c^{A\dagger}. \qquad (170)$$

In Eqs. (168), (169), and (170) the site indices have been suppressed for brevity. In terms of these bilinears we may write

$$\mathcal{H}_{\mathrm{SUSY}} = -2D \sum_n (\vec{J}_{n+1} \cdot \vec{J}_n + J_{n+1} J_n - J_n)$$

$$+ 2D \sum_n (\vec{K}_{n+1} \cdot \vec{K}_n + K_{n+1} K_n + K_n)$$

$$+ D \sum_n (M_{n+1}^{(1)\dagger} M_n^{(1)} + M_{n+1}^{(2)\dagger} M_n^{(2)} + \mathrm{H.c.})$$

$$+ D \sum_n (L_{n+1}^{(1)\dagger} L_n^{(1)} + L_{n+1}^{(2)\dagger} L_n^{(2)} + \mathrm{H.c.}). \qquad (171)$$

Here H.c. denotes Hermitian conjugate and $\vec{K}_{n+1} \cdot \vec{K}_n = K_{n+1}^z K_n^z - K_{n+1}^x K_n^x - K_{n+1}^y K_n^y$.

It is instructive to study the commutation relations for bilinears at the same site n (bilinears at different sites simply commute or anticommute). It is easy to verify that J_+, J_-, and J_z satisfy angular momentum or su(2) commutation relations and J commutes with the other three. Similarly K_+, K_-, and K_z satisfy the su(1,1) or hyperbolic angular momentum algebra—essentially the angular momentum algebra but with a sign change for the K_+, K_- commutator [39]. K commutes with the other three. The anticommutators of L_i, $L_i^\dagger$, M_i, and $M_i^\dagger$ are linear combinations of the K's and J's. The commutators of the J's or K's with the L's or M's are linear combinations of the L's and M's. Hence these bilinears constitute a superalgebra. The J's and K's are commuting elements of the superalgebra; the L's and M's, anticommuting elements. The superalgebra is called u(1,1–2). It includes the Lie algebras su(2) and su(1,1) as subalgebras.

Further insight into the superalgebra is obtained by considering the Hilbert space at a single site. This is a direct product of the four-dimensional fermion space and the infinite dimensional two-boson space. The fermion space may be decomposed into irreducible representations of the su(2) algebra. The fermion vacuum and the state with both R and A

fermions present constitute a doublet or spin one-half representation; the two states with one fermion present are singlets. The boson space similarly decomposes into an infinity of infinite dimensional irreducible representations of thesu(1,1) algebra.[5] The single site Hilbert space thus decomposes rather simply into irreducible representations of the direct sum of the su(2) and su(1,1) algebra. These subspaces do not constitute a representation of the whole superalgebra. The anticommuting elements mix different irreducible representations of su(2) and su(1,1). In particular they mix representations with different spins—a celebrated feature of supersymmetry. It is not difficult to decompose the single site Hilbert space into blocks irreducible under the superalgebra; however this would carry us too far afield. More details on the superalgebra are given in Ref. [26] and references therein.

Finally we define

$$\mathcal{J}_{\text{tot}} = \sum_n \mathcal{J}_n. \tag{172}$$

Here $\mathcal{J}$ denotes any element of the superalgebra such as J_+, K_z, L_1, etc. After some algebra we find

$$[\mathcal{H}_{\text{SUSY}}, \mathcal{J}_{\text{tot}}] = 0 \tag{173}$$

revealing the supersymmetry of the field theory formulation.

VII. SUMMARY AND CONCLUSION

Much of this paper is concerned with the behavior of the q model close to the critical point. To probe this behavior we imagine that a uniform load is applied to the top layer. The assumption of uniform load is for convenience; in the scaling limit the behavior of the load at sufficient depth is insensitive to the initial distribution. As the load propagates downward fluctuations develop in the distribution of load. Coppersmith *et al.* [4] studied the entire distribution of load at very great depth where it was presumed that a steady state had been reached. In contrast we study only the variance of the distribution of load but we analyze its evolution with depth. Our purpose is to study this evolution for all distributions of the fractions $P(f)$ particularly those close to the singular distribution (the critical point).

In Sec. II we consider the q model in $1+1$ dimensions without injection (the weight of the beads is neglected). In this case the average load does not vary with depth since the total load is the same in every layer; it is merely redistributed by the q-model dynamics. For the growth of the variance, by analogy to critical phenomena, we make the following hypotheses: For all distributions $P(f)$ except the singular dis-

tribution we posit that the variance will saturate at sufficient depth. Both the saturation depth and the saturated variance are expected to diverge as the distribution approaches the singular distribution. We introduce δ, a measure of the distance of a distribution $P(f)$ from the singular distribution, and conjecture that the saturation depth ξ_{corr} will diverge as $1/\delta^\varphi$; the saturated variance, as $1/\delta^\theta$. More specifically, we expect that close to the critical point the variance will have a scaling form, Eq. (7). For the singular distribution we expect that the variance will grow indefinitely as a power of the depth. Close to the critical point and at depths shallow compared to the saturation depth the variance should grow as it would right at the critical point. From this and from Eq. (7) we deduce a relationship between the critical exponents θ and φ and the exponent that describes the growth of the variance right at the critical point; namely we expect that at the critical point the variance will grow as $t^{\theta/\varphi}$. In Secs. II B and II C we derive an exact formula for the variance as a function of depth [Eq. (46)] and study its scaling limit ($t \gg 1$, $\delta \to 0$ but with $t\delta^\varphi$ arbitrary). These calculations bear out all the expectations enumerated above, provide the precise form of the scaling function [Eq. (50) and Fig. 4] and yield the exact exponents [Eq. (49)].

In Sec. III we characterize the critical point more fully by analyzing the evolution with depth of the entire distribution of load right at the critical point in $1+1$ dimensions. In the absence of injection the critical point is a simple model of random walkers that coalesce upon contact; hence it is quite straightforward to derive these results. We present them because they illuminate the results of the previous section. At large depth it is found that the distribution of load consists of a large spike at zero load together with a smooth part [Eqs. (73) and (76)]. It is overwhelmingly probable that the load on a bead is zero; most of the weight of the distribution is in the spike. The smooth part follows the anticipated scaling form [Eq. (53)]. Its width grows as the square root of the depth, consistent with the exponent found in Sec. II to describe the growth of the variance of load at the critical point.

In Sec. IV the effect of injection is included. For simplicity we consider only $1+1$ dimensions. We assume that the weights of the beads are independent and identically distributed random variables. The behavior of the mean load is still not very interesting. It grows linearly with depth [Eq. (77)]. Close to the critical point we conjecture that the variance will have the form Eq. (78). We are able to deduce all the exponents in Eq. (78) and to obtain some limiting behaviors of the scaling function through simple (nonrigourous) arguments. These conjectures are all verified by the exact calculation of Secs. IV A and IV B that provides the precise form of the scaling function [Eqs. (99), (102), and (103)] and yields all the exponents [Eqs. (80), (81), and (84)]. We find that beyond a crossover depth the variance (normalized by the squared mean) saturates. The saturation value and the crossover depth both diverge as the critical point is approached. At depths less than the crossover depth the variance grows as it would right at the critical point [Eq. (106)]. The behavior at the critical point has many crossovers if the weight of the beads is small compared to the applied load. In this case at first the variance grows as the square root of the

---

[5] Let $|n+m,n\rangle$ denote a state with $(n+m)$ R bosons and n A bosons on the site. The infinite dimensional subspace with m a fixed integer and $n=0,1,2,\ldots$, for $m \geq 0$, or $n=-m,-m+1,=m+2,\ldots$, for $m<0$, is invariant under the four K operators. These subspaces corresponding to different values of m constitute the irreducible representations of the su(1,1) algebra.

depth as it was found to do in Sec. II in the absence of injection. At greater depths there are crossovers to growth as t and $t^{5/2}$, as first the effects of large rare fluctuations in the weight of a bead and then mean injection assert themselves. Ultimately at the critical point the variance grows with the 5/2 exponent but the depth at which this behavior sets in can be very great if the mean injection is small. This depth diverges as $\langle I \rangle^{-4/3}$. The crossover exponent 4/3, deduced by simple arguments and then via exact calculation in Sec. IV, agrees with the value previously obtained by a different method by Majumdar and Sire [28]. In their work Majumdar and Sire only study the behavior right at the critical point. However at this point they calculate the dynamics of the entire distribution of load whereas we study only the variance.

In Sec. V we turn to the q-model in $D+1$ dimensions. For simplicity we neglect injection in this section. We find that right at the critical point the variance grows as a power of depth in all dimensions except two [Eq. (137)]. The power is given by $D/2$ for $D<2$. For all dimensions above two the growth is linear. This shows that $D=2$ is the upper critical dimension for this problem. For $D=2$ we find a linear growth of the variance tempered by a log factor as might be expected at the critical dimension.

An intriguing feature of the critical behavior we obtain is that it is exhibited at all. For ordinary continuous phase transitions the renormalization group provides a framework to understand the critical behavior. We are not aware of any such framework for the q model.

Random critical points are notoriously difficult to analyze in general. The feature that allows us to analyze the q model is that the two point load correlation function [defined by Eqs. (8) and (114)] evolves with depth according to a simple linear equation. In Sec. II we analyze the evolution by expanding in the eigenvectors of an appropriate linear operator. There are some subtleties posed by the non-Hermiticity of the linear operator, making it necessary to prove that its eigenvectors are complete (further complicated by the infinite dimensionality of the vector space). Nonetheless we like this approach because it parallels transfer matrix methods used for equilibrium critical phenomena. We find that the large depth scaling behavior is controlled by the low energy long wavelength eigenfunctions of the non-Hermitian "Hamiltonian." Another virtue of this approach is that with about the same effort it yields both the variance and the correlation functions. However we have left analysis of the correlation functions open for later work. Here we focus entirely on the variance of the load. In Sec. V we analyze the variance using another technique based on transform methods.

Our analysis, neglecting injection, confirms that the q model has essentially no horizontal correlations in the steady state for any distribution except the singular. This agrees with experiments on bead packs. The bulk of our results however are concerned with the q model close to the critical point. Bead pack experiments such as those of Ref. [12] appear to be far from the critical point. We estimate $\delta \approx 0.5$ for this experiment. It is not obvious how to tune the parameter for bead packs to access the critical behavior we analyze

here. Claudin *et al.* have also studied the horizontal steady state correlations of the q model without injection away from the critical point [8]. They employ a continuum limit and arrive at conclusions similar to Eq. (19) in Sec. II B. The main focus of their work however is to explore a tensor model of stress propagation in granular matter, intended to supplant the q model.

Interpreted in terms of river networks our results show that allowing a small amount of river splitting in a Scheidegger network introduces a length scale in the vertical direction. On sufficiently long length scales such a network is not scale invariant. This resembles the finding of Narayan and Fisher [20]. In their model too there was a parameter that controlled river splitting. Their networks were not scale invariant unless river splitting was tuned to zero. However their model appears to be in a different universality class as its vertical correlation exponent is different from the value $\varphi=2$ we obtain here in Sec. II. Presumably the difference is because their rule for stream splitting was nonlocal and depended on the entire history of the network upstream from the split.

Taken together with the model of Narayan and Fisher it appears that river splitting is a perturbation that spoils the scale invariance of river networks. It is therefore interesting to ask whether such networks exist in Nature. River deltas are one possibility. Traced backwards they may constitute networks of merging streams that occasionally split. Even for river basins it might be interesting to examine the extent to which streams split. In this context it is worth noting that some of the data against which river scaling laws are tested are based not on actual maps of the river network but on networks that are indirectly inferred according to certain rules from digital elevation data obtained from satellite images. The rules by which the network is inferred from the elevation maps exclude the possibility of splitting [18].

In summary the q model is rich in applications and behavior and yet analytically tractable by elementary means, a combination of circumstances that invites further exploration. Among the many problems that remain open we conclude by mentioning two: For the q model beyond the saturation depth there is no correlation in the horizontal direction but in the vertical direction there are very strong and long ranged correlations [40]. We have not obtained the precise form of these vertical correlations for the q model either in steady state or at the critical point. It would be very interesting (and straightforward) to obtain these forms and the crossover between them. Second it would be interesting to obtain the dynamics of the entire distribution of load near the critical point. We have not attempted to do this except right at the critical point.

A natural scaling hypothesis is that the full distribution of load, neglecting injection, will be of the form

$$\Pi(w,t,\delta)=w^{-\tau}\Pi(w\delta^{1/\sigma},t\delta^{\nu z}). \qquad (174)$$

The exponents in Eq. (174) are $\tau=2$, $\nu z=2$, and $\sigma=1$. Their values are fixed by our result for the variance away from the critical point derived in Sec. II and the result for the entire distribution at the critical point $\delta=0$ derived in Sec.

III. We also know that for $x \to 0$ and $y \to 0$, the presently unknown function $\mathcal{Q}$ has the asymptotic behavior

$$\mathcal{Q}(x,y) \approx \frac{4}{\sqrt{\pi}} \frac{x}{y^{3/2}} e^{-x^2/y} \qquad (175)$$

to be consistent with the critical point distribution [Eq. (73)] derived in Sec. III.

In the second part of this paper we turn to chiral wave models that are believed to describe the surface electronic states of a quantum Hall multilayer. In Sec. VI A we discuss circumstances under which the quantum network model of Saul, Kardar, and Read (described in the introduction) is equivalent to the q model. In Sec. VI B we compare known results about the behavior of the q model to a continuum chiral wave model that cannot be mapped onto a q model under any circumstance. The two are found to behave in qualitatively similar ways.

A circumstance under which the mapping to the q model is not useful is when periodic boundary conditions must be imposed in the chiral direction. Physically this is because of the interference of electron paths that wind around the quantum Hall multilayer. Such long range interference cannot be captured by the classical q model. In this phase-coherent or mesoscopic regime, the chiral wave model has been studied via a mapping to a supersymmetric spin model [23,26]. In Sec. VI C we derive this mapping in a way that emphasizes boundary conditions. Our derivation makes use of operator methods and is hence more elementary than the derivation of Ref. [26] that makes use of mixed functional integrals over Grassman and bosonic variables. We do not attempt further analysis of the superspin model here; the interested reader should consult papers on multilayer transport, particularly Refs. [41] and [23] that provide a nice overview of the early work on this problem.

Mappings to superspin models have been useful not only in the study of the quantum Hall multilayer but have also recently lead to new nonperturbative results and insights into other important problems of electron localization [35–37]. Hence it is hoped that our derivation, with its emphasis on boundary conditions and use of elementary operator methods, will be of interest in this general context.

Note added. While writing this paper we learned of an e-print by Rajesh and Majumdar on spatiotemporal correlations in the Takayasu model and the q model [42]. These authors derive many interesting results complementary to ours. In this paper we concentrate on the behavior close to the critical point. For the q model, Rajesh and Majumdar concentrate on length scales long compared to our vertical correlation length ξ_{corr}; the crossovers and scaling functions that we study are transients that are invisible in their asymptotic formulas. On the other hand they have derived both vertical and horizontal load correlation functions; this paper is limited (in practice but not in principle) to the study of the variance of load. Among their interesting findings (i) they find power law correlations in the vertical direction both at the critical point and away from it addressing in part a

question raised above; and (ii) they emphasize the interesting structure of the horizontal correlation function, including injection, at great depth.

Although the goals are a bit different, there are points of intersection between the two papers with regard to technique. Rajesh and Majumdar too exploit the linearity of the relation that describes the evolution of the correlations with depth and solve it using the method of Sec. V. An overlapping result is a formula for the variance at the critical point in $1 + 1$ dimensions including injection. At the large depths studied by Rajesh and Majumdar the last term in our Eq. (106) should dominate. Rajesh and Majumdar obtain the same exponent 5/2 and the same numerical prefactor $16/15\sqrt{\pi}$ providing a nice check on both calculations.

APPENDIX A: PROOF OF COMPLETENESS

First let us recall the principles of biorthogonal expansion (see, for example, Ref. [27], p. 884). We discuss the simplest case of a finite $N \times N$ dimensional non-Hermitian matrix H_{mn}. Consider its eigenvectors

$$\sum_n H_{mn} \phi_n^\lambda = \lambda \phi_m^\lambda. \qquad (A1)$$

In context of biorthogonal expansion these eigenvectors are called the right eigenvectors. For simplicity we will assume that the right eigenvalues are nondegenerate in this case. The bad news regarding the right eigenvectors is: (i) λ may be complex. (ii) There is no guarantee that there are N eigenvectors (needed to span the vector space). (iii) Eigenvectors corresponding to different eigenvalues are not necessarily orthogonal.

Now consider the left eigenvectors, defined as the eigenvectors of $H^\dagger$. (i) If λ is a right eigenvalue then λ^* is a left eigenvalue (Proof: The coefficients for the characteristic polynomials of H and $H^\dagger$ are complex conjugates of one another). (ii) There are as many left eigenvectors as right. (iii) Left eigenvectors are orthogonal to right eigenvectors.

The last point merits elaboration. Let ψ_n^λ denote the left eigenvector with left eigenvalue λ^*. Thus

$$\sum_n H_{mn}^\dagger \psi_n^\lambda = \lambda^* \psi_m^\lambda. \qquad (A2)$$

According to (iii) above

$$\sum_n (\psi_n^\lambda)^* \phi_n^{\lambda'} = \delta_{\lambda\lambda'}. \tag{A3}$$

Equation (A3) is the *biorthogonality* relation. It may be proved by noting

$$\sum_{mn} (\psi_n^\lambda)^* H_{nm} \phi_m^{\lambda'} = \lambda \sum_n (\psi_n^\lambda)^* \phi_n^{\lambda'}$$

$$= \lambda' \sum_n (\psi_n^\lambda)^* \phi_n^{\lambda'}, \tag{A4}$$

whence $\sum_n (\psi_n^\lambda)^* \phi_n^{\lambda'} = 0$ for $\lambda \neq \lambda'$.

In general there is no guarantee of completeness, but in this case assume that N eigenvectors have been found. Then we can prove the *completeness* relation

$$\sum_\lambda (\psi_m^\lambda)^* \phi_n^\lambda = \delta_{mn}. \tag{A5}$$

The proof follows from the observation that if there are N eigenvectors, any vector a_n may be expanded as

$$a_n = \sum_\lambda a_\lambda \phi_n^\lambda. \tag{A6}$$

Completeness then follows from biorthogonality, Eq. (A3).

The problem in Sec. II B presents some complications not present in the pedagogical discussion above. Among them are degeneracy, an infinite dimensional vector space and a continuous spectrum. Nonetheless the broad strategy is the same. In Sec. II B we found left and right eigenvectors and we conjectured biorthogonality and completeness relations. To justify the analysis of Sec. II B we must prove the completeness relation. That is the purpose of this Appendix. Note that we cannot simply assume completeness is true—because the matrix H is non-Hermitian there are no theorems to guarantee it. Nor can we prove completeness by counting eigenvectors as in the finite dimensional discussion above.

The proof of completeness is remarkably simple and direct. We substitute the exact expressions for $\psi_m^{(\pm)k}$ and $\phi_n^{(\pm)k}$ that we have derived, Eqs. (28), (31), (33), and (34), on the right hand side of Eq. (36) and verify the completeness relation by explicit evaluation of the integral. There are nine cases to consider corresponding to $n=0, n>0, n<0$ and $m=0, m<0, m>0$.

For illustration we analyze the case of $n=0, m=0$. We must evaluate

$$\frac{2}{\pi} \int_0^\pi dk \, \mathcal{A}^*(k) A(k), \tag{A7}$$

where $\mathcal{A}(k)$ and $A(k)$ are as given in Eqs. (30) and (35). Since the integrand is symmetric in k we extend the range of integration from $-\pi$ to π and substitute $z \to e^{ik}$ to obtain a contour integral about the unit circle
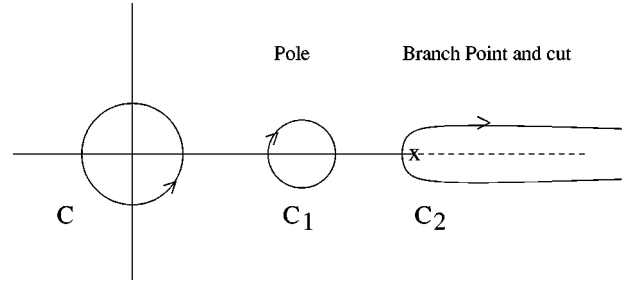

FIG. 10. Contours for inverting the z transform.

$$\oint \frac{dz}{2\pi i} \frac{1}{z} \frac{(1-\epsilon)(z+1)^2}{\epsilon^2(z-1)^2 - (1-\epsilon)^2(z+1)^2}. \tag{A8}$$

Evaluation via Cauchy's theorem reveals that the integral equals one as required for completeness.

The remaining eight cases also succumb to this method of analysis.

APPENDIX B: INVERSE z TRANSFORM

Consider the series $f(t)$, $t=0,1,2,\ldots$. Its z transform is defined as

$$f(z) = \sum_{t=0}^\infty f(t) z^t. \tag{B1}$$

Some z transforms can be inverted by inspection. For example the inverse transform of $(1-\alpha z)^{-1}$ is evidently

$$(1-\alpha z)^{-1} \to f(t) = \alpha^t. \tag{B2}$$

In other cases the inverse transform can be found by performing the complex integral

$$f(t) = \oint_C \frac{dz}{2\pi i} \frac{f(z)}{z^{t+1}}. \tag{B3}$$

The contour C must enclose the origin but no singularities of $f(z)$.

For illustration let us analyze

$$f(z) = (1-z)^{-1/2} (1-\alpha z)^{-1} \tag{B4}$$

needed to go from Eq. (43) to Eq. (44) in Sec. II B. Here $\alpha > 1$. $f(z)$ has a pole at $1/\alpha$ and a branch cut at $z=1$ (see Fig. 10). We deform the contour C that encloses the origin to contours C_1 and C_2 that encircle the pole and pass above and below the branch cut. Hence obtain

$$f(t) = \sqrt{\frac{\alpha}{\alpha-1}} \alpha^t - \frac{1}{\alpha\pi} \int_1^\infty dx (x-1)^{-1/2} \frac{1}{x^{t+1}} \left(x - \frac{1}{\alpha}\right)^{-1}. \tag{B5}$$

The first term is the contribution of the pole; the second, of the branch cut.

APPENDIX C: ASYMPTOTICS OF $\Phi_n(u)$

The asymptotics of the functions $\Phi_n(u)$ defined by Eq. (103) are needed to obtain the asymptotic behavior of the scaling functions in Secs. II C and IV B.

The large u behavior poses no difficulty. Evidently

$$\Phi_n(u) \approx \frac{\sqrt{\pi}}{2} \frac{1}{\sqrt{u}} \quad \text{as} \quad u \to \infty \tag{C1}$$

for all n. The small u behavior is a bit more subtle. Moreover, it turns out that due to cancellations we will need as many as five or six terms in the small u series for Φ_n to obtain the leading behavior of the scaling functions.

For definiteness consider the small u behavior of

$$\Phi_1(u) = \int_0^\infty ds \, \frac{e^{-us^2}}{(1+s^2)}. \tag{C2}$$

The leading term is obtained by setting $u=0$,

$$\Phi_1(0) = \frac{\pi}{2}. \tag{C3}$$

To obtain the next term it is tempting to expand the integrand in powers of u but this leads to divergent integrals. The divergence signals that the asymptotic series is not a simple power series in u.

It turns out the next term goes as $\sqrt{u}$. To show this, and to efficiently obtain many more terms in the series, consider

$$g(x) = \int_0^\infty ds \, \frac{e^{-x^2 s^2}}{(1+s^2)}. \tag{C4}$$

We will show that $g(x)$ is regular about $x=0$ and that its asymptotic behavior is a simple power series. To this end we observe that $g(x)$ obeys the first order differential equation

$$\frac{d}{dx} g - 2xg(x) + \sqrt{\pi} = 0. \tag{C5}$$

$x=0$ is a regular point for this equation; hence we attempt a series solution

$$g(x) = b_0 + b_1 x + b_2 x^2 + \cdots. \tag{C6}$$

We find $b_1 = -\sqrt{\pi}$ and the simple recurrence relation

$$b_n = \frac{2}{n} b_{n-2}. \tag{C7}$$

Evidently $b_0 = g(0) = \pi/2$. Hence we obtain the asymptotic series

$$g(x) = \frac{\pi}{2} - \sqrt{\pi}x + \frac{\pi}{2}x^2 - \frac{2}{3}\sqrt{\pi}x^3 + \frac{\pi}{4}x^4 - \frac{4}{15}\sqrt{\pi}x^5 + \cdots. \tag{C8}$$

Substituting $x \to \sqrt{u}$ we conclude

$$\Phi_1(u) = \frac{\pi}{2} - \sqrt{\pi}u^{1/2} + \frac{\pi}{2}u - \frac{2}{3}\sqrt{\pi}u^{3/2} + \frac{\pi}{4}u^2 - \frac{4}{15}\sqrt{\pi}u^{5/2}$$
$$+ \cdots \tag{C9}$$

for small u. Similarly

$$\Phi_2(u) = \frac{\pi}{4} - \frac{\pi}{4}u + \frac{2}{3}\sqrt{\pi}u^{3/2} - \frac{3}{8}\pi u^2 + \frac{8}{15}\sqrt{\pi}u^{5/2} + \cdots$$

$$\Phi_3(u) = \frac{3\pi}{16} - \frac{\pi}{16}u + \frac{3\pi}{32}u^2 - \frac{4}{15}\sqrt{\pi}u^{5/2} + \cdots. \tag{C10}$$

APPENDIX D: LATTICE GREEN'S FUNCTION

1. Two dimensions

Consider the Green's function in two dimensions for the lattice Schrödinger equation discussed in Sec. V A. The real space Green's function at the origin is given by

$$\mathcal{G}(E) = \int_{-\pi}^{\pi} \frac{dk}{2\pi} \int_{-\pi}^{\pi} \frac{dp}{2\pi} \left\{ E - \frac{1}{4}(1+\cos p)(1+\cos k) \right\}^{-1} \tag{D1}$$

[cf. Eqs. (121) and (128)]. We consider real $E>1$. In this appendix we show that

$$\mathcal{G}(E) = \frac{2}{\pi E} K\left(\frac{1}{\sqrt{E}}\right); \tag{D2}$$

here K is a complete elliptic integral of the first kind. From the well-documented properties of these integrals or by direct analysis of Eq. (D8) below it follows that as $E \to 1^+$

$$\mathcal{G}(E) \approx \frac{1}{\pi} \ln \frac{1}{E-1}. \tag{D3}$$

In Sec. V C we are interested in the behavior of $G(z)$, Eq. (131), as the real variable $z \to 1^-$. Comparing Eqs. (131) to (D1) we see that

$$G(z) = \frac{1}{z} \mathcal{G}\left(E \to \frac{1}{z}\right). \tag{D4}$$

Hence the singularity of $G(z)$ as $z \to 1$ is

$$G(z) = -\frac{1}{\pi} \ln(1-z). \tag{D5}$$

Equation (D5) is the main result of this section of the Appendix.

To demonstrate Eq. (D2) we regard p as a complex variable $p \to x + iy$. The integral over p in Eq. (D1) may be regarded as an integral around the contour sketched in Fig. 11 since the two vertical segments cancel by the periodicity of the integrand and the horizontal segment at infinity makes no
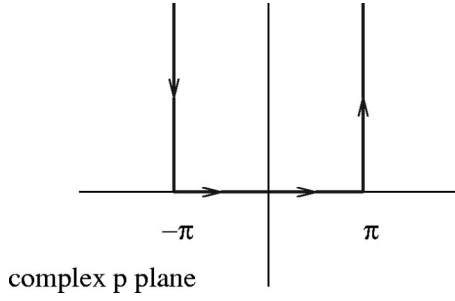
FIG. 11. Contour for evaluation of two-dimensional Green's function.

contribution because the integrand vanishes along it. The integrand in Eq. (D1) has a simple pole at $p = iy$, where y satisfies

$$\cosh\left(\frac{y}{2}\right) = \frac{\sqrt{E}}{\cos(k/2)}, \tag{D6}$$

with residue

$$\left(iE\sqrt{1 - \frac{1}{E}\cos^2\frac{k}{2}}\right)^{-1}. \tag{D7}$$

Hence by Cauchy's theorem

$$\mathcal{G}(E) = \frac{1}{E}\int_{-\pi}^{\pi}\frac{dk}{2\pi}\left(1 - \frac{1}{E}\cos^2\frac{k}{2}\right)^{-1/2}. \tag{D8}$$

Comparing to the definition of the elliptic integral of the first kind

$$K(k) = \int_0^{\pi/2}d\theta(1 - k^2\sin^2\theta)^{-1/2} \tag{D9}$$

we obtain Eq. (D2).

2. Below two dimensions

In this section we analyze the singular behavior as $z \to 1$ of $G(z)$ in less than two dimensions. The approximate long wavelength expression for G, Eq. (133), provides a useful starting point.

To analyze the divergence in $D = 1$ we would note that the integrand in Eq. (133) is a sharply peaked Lorentzian. This justifies working to quadratic order in $S(\vec{p})$ and extending the range of integration (strictly confined to the Brillouin zone, $-\pi < p < \pi$ in one dimension) to $\pm\infty$. Result: $G(z) = (1-z)^{-1/2}$.

To continue this result to nonintegral D we use 't Hooft and Veltman's dimensional regularization trick [43]. We write

$$G(z) \approx \int_0^{\infty}ds\int\frac{d\vec{p}}{(2\pi)^D}\exp -s[(1-z)+\vec{p}^2]; \tag{D10}$$

extend the range of integration, outside the Brillouin zone and over all $\vec{p}$-space; and replace

$$\frac{d\vec{p}}{(2\pi)^D} \to \frac{\Omega_D}{(2\pi)^D}\int_0^{\infty}dp\, p^{D-1}, \tag{D11}$$

since the integrand in Eq. (D10) is isotropic in $\vec{p}$. Here $\Omega_D = 2\sqrt{\pi}^D/\Gamma(D/2)$ is the total solid angle in D dimensions (some familiar special cases: $\Omega_1 = 2, \Omega_2 = 2\pi, \Omega_3 = 4\pi, \Omega_4 = 2\pi^2$.) The result is

$$G(z) = \frac{\Gamma(1 - D/2)}{\sqrt{\pi}^D}(1 - z)^{D/2 - 1} \tag{D12}$$

for $D < 2$.

This analysis breaks down in two dimensions and higher because the integrand diverges as $\vec{p} \to \infty$. The divergence is an artifact of the quadratic approximation in Eq. (133) and of extending the integral outside the Brillouin zone. The spurious divergence is revealed in Eq. (D12) as a pole in the Gamma function factor as $D \to 2$.

APPENDIX E: ANALYSIS OF PARTITION FUNCTION

The purpose of this Appendix is to show that the partition functions for bosons and fermions cancel. Thus

$$\text{Tr}[S_F^R(T)]\text{Tr}[S_B^R(T)] = 1. \tag{E1}$$

A similar relation holds for the advanced bosons and fermions. We discuss the retarded case explicitly. For brevity the superscript R will be omitted.

We write the fermion S matrix as

$$S_F(t) = \exp\left(i\frac{\pi t}{T}\sum_n c_n^{\dagger}c_n\right)\mathcal{S}_F(t). \tag{E2}$$

$\mathcal{S}_F(t)$ is then governed by the Hamiltonian Eq. (146) without the extra term included in Eq. (153).

To make further progress we introduce $e_l^n(t)$, the solution to the Schrödinger Eq. (144)

$$-i\frac{\partial}{\partial t}e_l^n(t) = m_l(t)e_{l+1}^n(t) + m_{l-1}^*(t)e_{l-1}^n(t) \tag{E3}$$

subject to $e_l^n(t \to 0) = \delta_{nl}$.

The scattering formula

$$c_n\mathcal{S}_F(t) = \sum_l e_n^l(t)\mathcal{S}_F(t)c_l \tag{E4}$$

will prove very useful. To derive it, rewrite Eq. (E4) as

$$\mathcal{S}_F(t)^{-1}c_n\mathcal{S}_F(t) = \sum_l e_n^l(t)c_l \tag{E5}$$

and regard it as an ansatz with the functions $e_n^l(t)$ unspecified. Making use of Eqs. (147), (148), and (151), the t derivative of the left hand side is

$$\mathcal{S}_F(t)^{-1}\{m_n(t)c_{n+1}+m^*_{n-1}(t)c_{n-1}\}\mathcal{S}_F(t)$$

$$=\sum_l c_l\{m_l(t)e^l_{n+1}(t)+m^*_{l-1}(t)e^l_{n-1}(t)\}. \quad \text{(E6)}$$

To obtain the second line we have made use of the ansatz (E5). Comparing Eq. (E6) to the t derivative of the right hand side of Eq. (E5) we conclude that $e^l_n(t)$ does obey the Schrödinger Eq. (E3). This completes the proof of the scattering formula (E4).

Another relation that will prove useful is

$$\mathcal{S}_F(t)|0\rangle=|0\rangle. \quad \text{(E7)}$$

This follows because the Hamiltonian [Eq. (146)] annihilates the vacuum; $\mathcal{S}_F$ is the (chronologically ordered) exponential of the Hamiltonian.

Equipped with these results we write the fermion partition function as

$$Z_F(T)=\mathrm{Tr}\left\{\exp\left[i\pi\sum_n c^\dagger_n c_n\right]\mathcal{S}_F(T)\right\}$$

$$=\langle 0|\mathcal{S}_F(T)|0\rangle-\sum_n \langle 0|c_n\mathcal{S}_F(T)c^\dagger_n|0\rangle$$

$$+\frac{1}{2}\sum_{n_1,n_2}\langle 0|c_{n_1}c_{n_2}\mathcal{S}_F(T)c^\dagger_{n_2}c^\dagger_{n_1}|0\rangle$$

$$-\frac{1}{3!}\sum_{n_1,n_2,n_3}\langle 0|c_{n_1}c_{n_2}c_{n_3}\mathcal{S}_F(T)c^\dagger_{n_3}c^\dagger_{n_2}c^\dagger_{n_1}|0\rangle+\cdots.$$

$$\text{(E8)}$$

The trace is taken over the entire Fock space including states with different total numbers of fermions. The alternating signs are due to the factor $\exp[i\pi\Sigma_n c^\dagger_n c_n]$ in the trace. The factorials are because the sums over the site indices n_i are unrestricted; hence each state gets counted a multiple number of times.

We now shift the S matrix to the left using the scattering formula (E4), make use of the adjoint of Eq. (E7) and calculate the vacuum expectations of the fermion operators (Wick's theorem). The result for the second-order term is

$$Z_F(T)=\frac{1}{2}\left[\sum_n e^n_n(T)\right]^2-\frac{1}{2}\sum_{n_1,n_2}e^{n_2}_{n_1}(T)e^{n_1}_{n_2}(T)+(\text{others}).$$

$$\text{(E9)}$$

Figure 12(b) shows a diagrammatic representation of this term. Note that the diagram series for the partition function $Z_F(T)$ contains both connected and unconnected graphs. By familiar arguments [38] we can write

$$Z_F(T)=\exp[-\Omega(T)], \quad \text{(E10)}$$

where the "free energy" $\Omega(T)$ has the linked diagram expansion shown in Fig. 12(c).
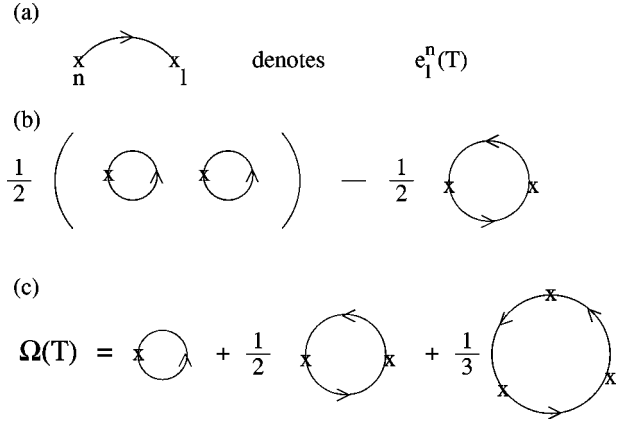

FIG. 12. Feynman diagrams for the partition function. (a) Diagram representation of the propagator $e^n_l(T)$. (b) Second-order diagrams for the partition function. (c) Lowest-order diagrams in the infinite series for the free energy.

We turn now to the boson partition function.
The boson scattering formula

$$b_n S_B(t)=\sum_l e^l_n(t)S_B(t)b_l \quad \text{(E11)}$$

can be proved in the same way as Eq. (E4). Equation (E7) remains true when we replace $\mathcal{S}_F\rightarrow S_B$.

The boson partition function is therefore given by

$$Z_B(T)=\mathrm{Tr}\{S_B(T)\}$$

$$=\langle 0|S_B(T)|0\rangle+\sum_n \langle 0|b_n S_B(T)b^\dagger_n|0\rangle$$

$$+\frac{1}{2!}\sum_{n_1,n_2}\langle 0|b_{n_1}b_{n_2}S_B(T)b^\dagger_{n_2}b^\dagger_{n_1}|0\rangle+\cdots.$$

$$\text{(E12)}$$

This equation resembles Eq. (E8) but there is an extra subtlety in the combinatoric factors. In the two-boson case, for example, for the off-diagonal terms $(n_1\neq n_2)$ the factor $(1/2!)$ is to offset double counting as in the fermion case. For the diagonal terms, that vanish in the fermion case, there is no double counting but the factor $(1/2!)$ is needed for normalization.

By shifting $S_B(T)$ to the left by use of the scattering formula we see that the series for $Z_B(T)$ is the same as for $Z_F(T)$ except for the minus signs. Hence

$$Z_B(T)=\exp[+\Omega(T)], \quad \text{(E13)}$$

where $\Omega(T)$ is defined by the diagram series in Fig. 12(c).

Equations (E10) and (E13) together lead to Eq. (E1), the result we sought to prove here.

[1] R. P. Feynman, R. B. Leighton, and M. Sands, *The Feynman Lectures on Physics* (Addison-Wesley, Reading, MA, 1965), Vol. 2, Chap. 12.

[2] A. E. Scheidegger, Bull. Intl. Assoc. Sci. Hydrol **12**, 15 (1967).

[3] H. Takayasu, Phys. Rev. Lett. **63**, 2563 (1989); H. Takayasu, I. Nishikawa, and H. Tasaki, Phys. Rev. A **37**, 3110 (1988).

[4] S. N. Coppersmith, C.-H. Liu, S. N. Majumdar, O. Narayan, and T. A. Witten, Phys. Rev. E **53**, 4673 (1996).

[5] D. Dhar and R. Ramaswamy, Phys. Rev. Lett. **63**, 1659 (1989).

[6] L. Saul, M. Kardar, and N. Read, Phys. Rev. A **45**, 8859 (1992).

[7] J. T. Chalker and A. Dohmen, Phys. Rev. Lett. **75**, 4496 (1995).

[8] P. Claudin, J. P. Bouchaud, M. E. Cates, and J. P. Wittmer, Phys. Rev. E **57**, 4441 (1998).

[9] For a review see B. I. Shraiman and E. D. Siggia, Nature (London) **405**, 639 (2000).

[10] H. M. Jaeger, S. R. Nagel, and R. P. Behringer, Rev. Mod. Phys. **68**, 1259 (1996); P. G. de Gennes, *ibid.* **71**, S374 (1999).

[11] C.-H. Liu, S. R. Nagel, D. A. Schecter, S. N. Coppersmith, S. N. Majumdar, O. Narayan, and T. A. Witten, Science **269**, 513 (1995).

[12] D. M. Mueth, H. M. Jaeger, and S. R. Nagel, Phys. Rev. E **57**, 3164 (1998).

[13] O. Narayan, e-print cond-mat/0004399.

[14] A. Liu and S. R. Nagel, Nature (London) **396**, 21 (1998).

[15] J. E. S. Socolar, Phys. Rev. E **57**, 3204 (1998).

[16] S. Kramer and M. Marder, Phys. Rev. Lett. **68**, 205 (1992).

[17] R. Leheny and S. R. Nagel, Phys. Rev. Lett. **71**, 1470 (1993).

[18] I. Rodriguez-Iturbe and A. Rinaldo, *Fractal River Basins: Chance and Self-Organization* (Cambridge University Press, Cambridge, UK, 1997).

[19] P. S. Dodds and D. H. Rothman, Phys. Rev. E **59**, 4865 (1999).

[20] O. Narayan and D. S. Fisher, Phys. Rev. B **48**, 7030 (1993).

[21] H. Stormer *et al.*, Phys. Rev. Lett. **56**, 85 (1986); D. P. Druist *et al.*, *ibid.* **80**, 365 (1998).

[22] L. Balents and M. P. A. Fisher, Phys. Rev. Lett. **76**, 2782 (1996).

[23] I. A. Gruzberg, N. Read, and S. Sachdev, Phys. Rev. B **55**, 10 593 (1997); **56**, 13 218 (1997).

[24] H. Mathur, Phys. Rev. Lett. **78**, 2429 (1997).

[25] Y.-K. Yu and H. Mathur, Phys. Rev. Lett. **81**, 3924 (1998).

[26] L. Balents, M. P. A. Fisher, and M. Zirnbauer, Nucl. Phys. B **483**, 601 (1996).

[27] P. M. Morse and H. Feshbach, *Methods of Theoretical Physics* (McGraw-Hill, New York, 1953), Vol. 1.

[28] S. N. Majumdar and C. Sire, Phys. Rev. Lett. **71**, 3729 (1993).

[29] S. N. Majumdar and D. A. Huse, Phys. Rev. E **52**, 270 (1995).

[30] R. Friedberg and Y.-K. Yu, Phys. Rev. E **49**, 5755 (1994).

[31] See, for example, M. Hamermesh, *Group Theory and its Application to Physical Problems* (Dover, New York, 1989), p. 313.

[32] A. A. Ovichinnikov and N. S. Erikhman, Zh. Éksp. Teor. Fiz. **67**, 1474 (1974) [JETP **40**, 733 (1974)]; A. Madhukar and W. Post, Phys. Rev. Lett. **39**, 1424 (1979); S. M. Girvin and G. D. Mahan, Phys. Rev. B **20**, 4896 (1979).

[33] J. P. Bouchaud, D. Touati, and D. Sornette, Phys. Rev. Lett. **68**, 1787 (1992).

[34] D. Cule and Y. Shapir, Phys. Rev. B **50**, 5119 (1994).

[35] J. B. Marston and S.-W. Tsai, Phys. Rev. Lett. **82**, 4906 (1999); T. Senthil and M. P. A. Fisher, Phys. Rev. B **60**, 6893 (1999); I. A. Gruzberg, A. W. W. Ludwig, and N. Read, Phys. Rev. Lett. **82**, 4524 (1999).

[36] L. Balents and M. P. A. Fisher, Phys. Rev. B **56**, 12 970 (1997).

[37] H. Mathur, Phys. Rev. B **56**, 13 263 (1997).

[38] A. L. Fetter and J. D. Walecka, *Quantum Theory of Many Particle Systems* (McGraw-Hill, New York, 1971).

[39] D. Mattis, *The Theory of Magnetism* (Springer Verlag, Berlin, 1988), Vol. 1.

[40] S. R. Nagel (private communication).

[41] S. Cho, L. Balents, and M. P. A. Fisher, Phys. Rev. B **56**, 15 814 (1997).

[42] R. Rajesh and S. N. Majumdar, Phys. Rev. E **62**, 3186 (2000); e-print cond-mat/0004442.

[43] See, for example, M. Stone, *The Physics of Quantum Fields* (Springer, Berlin, 2000), Chap. 5.